Measurement, Volume 139, June 2019, pp. 387-402
DOI: 10.1016/j.measurement.2019.03.026

Advances in test and measurement of the interface adhesion and bond strengths in coating-substrate systems, emphasising blister and bulk techniques

Xiaomei Chen[1]*, Christopher Shaw[2], Len Gelman[3]and Kenneth T V Grattan[4]

1. Academy of Opto-Electronics, Chinese Academy of Sciences, Haidian District, Beijing 100094, China

2. Surface Engineering and Precision Institute, Cranfield University, Cranfield, Bedfordshire MK43 0AL, UK

3. Centre for Efficiency &Performance Engineering, University of Huddersfield, Huddersfield HD1 3DH, UK

4. School of Mathematics, Computer Science and Engineering, City University London, London EC1V 0HB, UK

* xiaomei.chen@aoe.ac.cn

Abstract

In this paper, recent advances in the minimum-destructive testing of the adhesion of coating-substrate systems are reviewed, focusing on key areas such as micro- and nano-scale levels of indentation, scratch, laser-induced wave shock, as well as blister and buckle. Along with adhesion failure tests, the latest and most extensive applications of the adhesion test methods in nano-, micro- and bulk-coating technology and the associated techniques to determine the minimum damage defects left on the coatings are discussed and reviewed.

Keywords: interface adhesion, bond strength; coating-substrate system; minimum-destructive testing.

1. Introduction

Coating-substrate systems embrace a wide range of diverse materials, including metals, metal alloys and compounds, polymers, organics and composites. The coating thicknesses produced range from sub-nanometre thin films (such as few-layer 2D-graphene) through to hundreds of microns, and rely on the specific physical properties of the materials. Such coatings play important roles in protecting surfaces in the aerospace and automobile industries, as well as in the Microelectronics and Nano-technological fabrication industries, such as the Micro Electromechanical Systems (MEMS).

Coating adhesion failure will occur as a result of various internal or external forces. These include mechanical stress, environment-induced thermal stress and corrosion as the typical main causes of adhesion failure. The adhesion testing of a coating to a substrate is of great significance, as coating failure is usually a long and slow process for in-service coating systems and therefore coating adhesion tests can help to accelerate and actively promote the de-adhesion and delamination process. The adhesion strength measurement can provide a guideline in the design and option of coating methods and material pairs for a coating-substrate system. Graystone and Kennedy [1] have previously reviewed a range of non-destructive techniques for coating adhesion detection and analysis. They proposed that if only a minimum localized coating or substrate was destroyed or ruptured during the testing process, the method was effectively a type of non-destructive testing (NDT) technique. Testing techniques of this kind should include mechanical-based micro-indentation testing, micro-scratch testing (using both stylus and pulsed infrared laser), laser induced shock spallation, blister and buckle testing, topics which this paper will review. Although blister and buckle testing has been implemented for decades, it deserves revisiting because of its more recent extensive application in

graphene-based 2D nano-materials. Except for the laser induced shock spallation, the other aforementioned testing techniques have also advanced to be generally applied for bulk coating-substrate systems and thin film nanomaterial coatings, as reviewed earlier by Volinsky et al [2] and later by Chen et al [3]. These reviews briefly introduced adhesion testing nevertheless highlighted theoretical modelling and analytical methods of adhesion. The mathematical models in these reviews are classic and as such do not require repetition in this present review. On the other hand, the rapid advances in technology warrant that the latest applications of adhesion testing are needed to be included in this review paper. Apart from non-destructive testing, the minimum physical defect phenomena left on the coatings examined are micro- and nano-indentations, pile-ups, cracks, scratches, chips, blisters, bulges and buckles, for example. Associated with these local damage defects, many different measurement, detection and characterization techniques have been employed. These include acoustic emission (AE) detection, thermal wave imaging and infrared thermography imaging, laser interferometry, raster-scanning microscopy techniques such as atomic-force microscopy (AFM), acoustic probe microscopy (APM), scanning electron microscopy (SEM), scanning electrochemical microscopy (SECM) and Raman spectroscopy. This range of testing methods and measurement techniques will form the basis of this review.

2. Micro- and Nano-indentation testing

Micro-hardness testers or indenter testers were developed historically for measuring surface hardness, Young's modulus of elasticity and other material properties [4] by continuously recording the force and the indentation depth. The International Organisation for Standardization (ISO) has specified this approach for coating testing, especially for nano- and micro-scale thin films, which include metallic, non-metallic and organic materials [5]. Graystone and Kennedy suggested that good adhesion at the interface is indicated by a smooth transition from coating to substrate (or primer) on the indentation profile, whereas poor adhesion will show non-uniformity. From the reviewed papers in this section, we have noticed the fact that the micro-hardness tester can provide the quantitative, semi-quantitative or qualitative measurement of adhesion needed, based on the degree of influence of the indenter on the rate of change of load with penetration depth.

According to indenter tip positions, indentations can be classified as: the interfacial indentation (Fig.1), coating surface indentation in the direction normal to the coating and substrate shown in Fig.2 (a) and on cross-sectional indentation on the substrate near to the interface shown in Fig.2 (b). Various indenter tip geometries such as circular cone (Rockwell) [6], triangular pyramid (Berkovich) [7], rhombic pyramid (Knoop) [8]and right pyramid (Vickers) [9] have been implemented historically.

The interfacial indentation testing has been shown to be particularly effective for the measurement of the adhesion strength of a brittle coating on a ductile or a brittle substrate. Based on Vickers hardness testing and the attached/separated optical microscope, the interfacial indentation test activities headed by Yamazaki et al [10][11], have led to the release of two ISO standards in the adhesion of thermal spaying coatings on bulk materials [12][13]. In reference [12], the adhesion is classified by the critical indentation force: the greater the critical indentation force, the higher the adhesion strength. It stipulates the criteria of interfacial crack initiation and the critical indentation force. The interfacial crack initiation is defined by the crack length greater than 50 μm, and the critical indentation force is defined by the maximum indentation force which induces the interfacial crack initiation with visible cracking frequency (*CF*) less than 50%. The *CF* is given by

$$CF = N_c/N_t \tag{1}$$

Where N_c is the number of indentations with visible cracking, N_t is the total number of indentation. The reference [13] recommends to quantitively evaluate adhesion of thermal spray ceramic coatings using interfacial toughness K_{IFC}. It is given by

$$K_{\mathrm{IFC}} = \frac{\eta}{\sqrt{2\pi}} \cdot \frac{F}{a\sqrt{c}} \cdot \cosh(\pi\varepsilon) \tag{2}$$

where c is the mean value of half crack length, a is the diagonal half-length of impression parallel to the interface, η is a constant (0.081), F is the test force. The bimaterial constant ε is defined as

$$\varepsilon = \frac{1}{2\pi} \ln \left(\frac{(3-\nu_1)E_2 + (1+\nu_2)E_1}{(3-\nu_2)E_1 + (1+\nu_1)E_2} \right) \quad (3)$$

where E_1 and ν_1 are the Young's modulus and Poisson's ratio of ceramic coating, respectively; and E_2 and ν_2 are the Young's modulus and Poisson's ratio of substrates, respectively. Equation (2) indicates that the shorter the crack length is, the higher the coating interfacial toughness or adhesion strength.

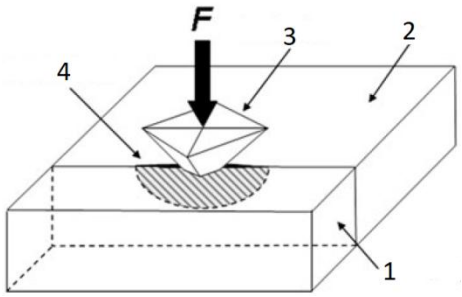

Fig.1 Schematic illustration of an interfacial indentation test by use of a Vickers indenter [12], where 1-coating; 2-substrate; 3-indenter; 4 interfacial crack.

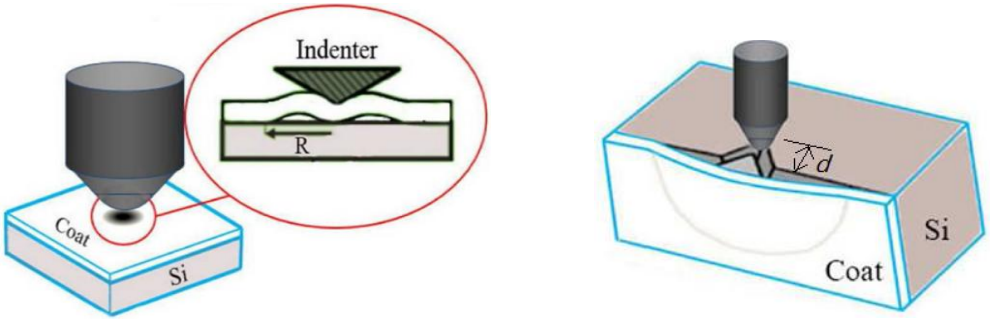

(a) (b)

Fig.2 Schematic configuration of indentation in (a) normal direction of coating-substrate interface and (b) cross-section[14], where R is the radius of buckle around the indenter, d is the distance of indenter tip away from the interface.

The coating surface indentation and cross-sectional indentation are more effective for the adhesion strength measurement of ductile films on brittle substrates. On recently investigating the effect of thickness on adhesion strength of ductile TiW thin films to brittle single crystal silicon wafers, Roshanghias et al [14] found that cross-sectional nano-indentation resulted in cracking similar to that shown in Fig.*1*, whilst normal direction nano-indentation induced blisters. After indentation testing, this study used focused ion beam and transmission electron microscopy (TEM) techniques to evaluate the adhesion.

Indentation-based stress, adhesion energy or other quantitative and semi-quantitative analysis models have been implemented for determining the adhesion and interfacial toughness of the thin coatings [15][16], especially by finite element modelling (FEM) [17][18][19]. The models have been established in close relation with the loaded forces and detected indentation-induced crack geometry parameters, as overviewed by Chen [20]. For the qualitative analysis of the adhesion of hard and brittle thin coatings, ISO have updated one evaluation standard document based on Rockwell indentation testing [21] normal to the coating-substrate interface, where the adhesion cracking and delamination is classified by four qualities, as determined by crack and delamination observations from optical microscopy.

Other examples of surface inspection and morphology analysis techniques being employed, are 3D images raster-scanned by SEM, TEM [22][23], and AFM [24][25]. In some examples, specialized techniques have

been integrated into the indenter itself. These include digital speckle pattern interferometry [26][27] and capacitive plate transducers [28] which measure the local displacement or penetrating depth of the indentation field generated by the tester. Another example of this is where the indentation damage effects were also measured by an indenter equipped with an AE sensor [29][30].

Interfacial indentation testing has recently been applied for determining the interface toughness of coatings obtained by vacuum plasma spray (VPS) [31], thermal barrier coating (TBC) [32], arc-ion plating [33], and cold-sprayed coating [34] techniques. The indentation methods have also been applied in composites [35] and polymer materials [36].

Annamalai et al [37] have exploited nano-indentation to tailor the surface ripples using an AFM cantilever tip as the nano-indenter in bilayer graphene which explored a novel fabrication of flexible electronic devices and strain sensors from graphene. Suk et al [38] recently used nano-indentation testing to look at the adhesion interactions of graphene when it was transferred onto the SiO_2 substrate. The nano-indenter was integrated with a capacitive MEMS force sensor to acquire the traction-separation interaction between the SiO_2 and graphene interfaces as well as the SiO_2 and graphene pair and diamond indenter tip schematically shown in

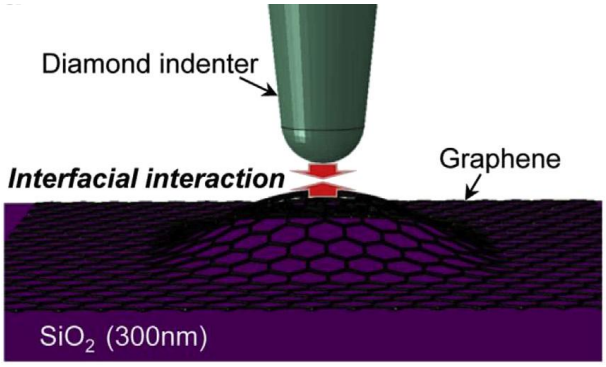

Fig.3. The classic Hertz, Johnson-Kendal-Roberts (JKR) and Derjaguin-Muller-Toporov (DMT) contact mechanics models were utilised to convert the mapped force profile into the adhesion energies. Other researchers have used AFM cantilever tips of different materials and shapes as the nano-indenter so as it approaches or moves away from the graphene, the measured resultant forces can be converted to the adhesion energies. The graphene was either in the form of a few layers as a free-standing beam [39] or on a metallic substrate [40][41][42].

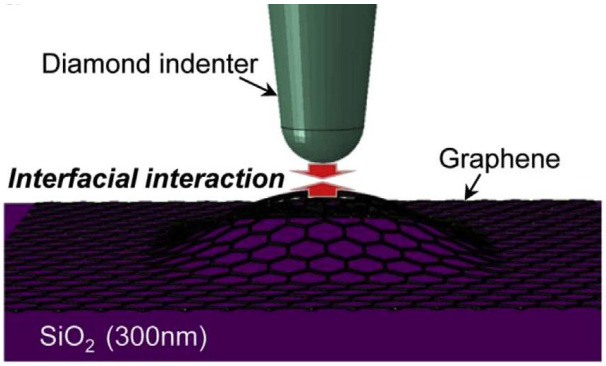

Fig.3 Schematic sketch of nano-indentation on graphene on silicon dioxide [38]

These aforementioned indentation procedures represent one-cycle loading and unloading tests. It should be emphasised that irrespective of the use of nano-indentation (load scale: 10 μN~10 mN) or micro-indentation testing, multi-cyclic indentation tests are always conducted for selected, specialist thin films [43][44].

3. Micro- and nano-scratch testing

Scratch testing involves applying an increasing force normally using a diamond stylus or indenter while the sample is moved tangentially with a frictional force. Both normal load and frictional force are simultaneously measured by the force sensors; the indentation depth and lateral displacement can be recorded as well. Eventually the resulting stresses cause chipping, flaking or cracking of the coatings on substrates, as illustrated by *Fig.4*. A sharp diamond stylus is more suitable for soft coatings on hard substrates, and a ball shaped indenter is often used for hard coatings [45]. The critical load *L*c, is the minimum load that causes a failure event. If the critical load is for a particular product, for example a scratch test, keeping the applied force below the critical load can be useful to create a 'pass/fail' criterion for adhesion strength and deformation behaviour in a quality control test, recommended by the BS 1071-3:2005(E) [46].

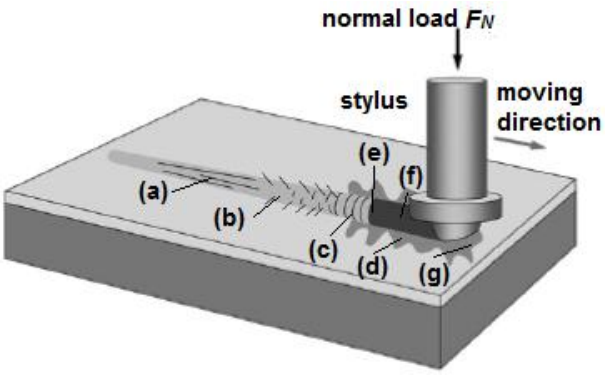

Fig.4 Schematic of scratch coating adhesion testing method modified from [45]: the surface cracks occur in the scratch test which can be characterized as (a) scratch, (b) angular scratch, (c) circular cracks, (d) coating chipping and spalling, (e) coating breakthrough, (f) exposed substrate, and (g) coating pile-up.

The coating failures in the scratch test are a complex combination of elastic-plastic indentation stress, frictional stress and residual stress in the coatings. Therefore, the scratch test can be regarded as a semi-quantitative adhesion test method due to the critical load measurement being related to these interior and exterior parameters [47]. The loading rate, scratching speed, indenter tip radius, indenter abrasion and testing-machine stiffness are the interior factors, while the coating-substrate system properties are the main Exterior Factors. The use of the Finite Element Method (FEM) has regularly been shown as a forceful tool in 3D CAD sketching to characterise the stresses, failure generation and fracture toughness of coating systems in the execution of the scratch test [48][49]. The critical load was detected by measuring the contact friction force variations [48] and plotting these as a function of the normal load. Historically, the AE sensors have been an integral part of the scratch testers for the detection of the initial fracture, this being done by analysing the plotted AE signal against the normal loading [50][51][52][54]. A sample plot of acoustic emission and frictional force against normal load, as well as critical load discrimination, is shown in *Fig.5*. Here, scratch tests coupled with AE detection were carried out on brittle coatings. The scratch process now described is defined as a mechanical deformation process: the diamond indenter moves across the surface of the specimen and a groove is formed. Different types of scratch damage have been observed in different materials. The relationship between the AE signals and scratch damage has been examined and the results show that the typical AE signals from the scratch process of the coatings are composed of continuous waveforms and bursts with high amplitude, but only acoustic emission bursts are observed in the scratch process of brittle coatings. It can be concluded that the detected bursts are generated due to the cracks whilst the continuous waveforms are generated due to ductile tearing, as illustrated in Fig.*5*. In addition, the AE amplitude, root mean square (RMS), kurtosis and mean frequency, change with increasing applied load and scratch velocity in different ways. The results of the AE mechanism are also further discussed by considering the effects due to stress, strain rate and temperature.

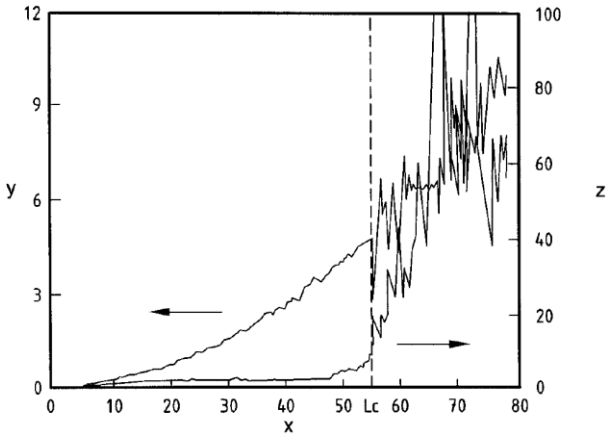

Fig.5 Example acoustic emission and frictional force vs. normal load, where X-normal load (N), Lc-critical normal load, Y-frictional force (N) and Z-acoustic emission (a.u.) [46]

The scratch patterns mapped by optical microscopy, SEM, AFM or X-ray photoelectron spectroscopy morphologically indicate and discriminate the failure types, such as stripping or flaking for soft coatings and buckling, and wedge spallation for hard coatings. The first failures are always determined from the photomicrographs, which are considered at the critical load.

Most research groups working in the field have combined frictional-force versus normal load, acoustic emission versus normal load, and photo-microscopy and raster-scan microscopy together in their scratch testing. Singh and Suri [53] have tested the adhesion and wear properties of magnetron sputtered NbN films on mild steel, stainless steel and high-speed steel substrates. The photographic evidence is depicted in the change of the scratch pattern change with increasing normal loads. Two critical loads have been defined – the first related to the initial cracking of coating and the second corresponding to observations of chipping and partial delamination so that the substrate beneath coating was exposed. During the scratch test, factors including the friction coefficient, the depth of indentation and the acoustic emission were plotted on the deposition spraying line as a function of the normal load and scratch distance. Some ten years ago, Gallego et al [54] characterized coating damage mechanisms by applying wavelet transformation of the AE signals during the scratch testing carried out, whilst illustrating the scratch cracks left on the corroded coating due to O and Cl diffusion along the interface of galvanised steel in SEM micrographs. As acoustic emission is a stochastic non-stationary process which involves elastic wave generation and propagation, they had found that the AE wavelet power spectrum reached its maximum when the coating failure occurs. Recently, Hassan et al [55] were able to identify the critical load for scratch an adhesion test process of Ni-based thin films by applying wavelet transform to the indentation depth versus scratch displacement curve generated.

In a way similar to micro-indentation testing, micro-scratch testing has been used extensively to evaluate the adhesion strength of hard thin coatings on a substrate. For example, Cai et al [56] recently investigated the adhesion and deformation of 21.3 μm thick NbC coatings on grey cast iron substrates using scratch testing. The critical load was determined from the AE intensity signals against the normal loads; radial (angular) cracks, lateral (circular) cracks, chipping and breakthrough along the scratch groove were identified in the high magnification of SEM micrographs, while the crack propagation along grain boundaries was observed in the ultrahigh magnification of SEM micrographs. Zawischa et al [57] have studied the adhesion failure of 1~3 μm super-hard carbon coatings on softer steel substrates by using scratch testing. Their view was that the adhesion failure of an ultra-hard thin coating on softer substrate is caused by plastic flow of the substrate and they calculated the stress distribution at the critical load based on Hertz contact mechanics model. Consequently, they found that adhesion failures depend on the critical load-induced maximum stress location, relative to the coating-substrate interface. The adhesion failure occurred in the form of angular cracks, circular hair cracks, wing-shape delamination, bending cracks and delamination at a bending crack.

What is notable about the result is that the authors quantified the adhesion failure size by means of micrographic image segmentation, and found its correlation to the calculated shear stresses at the interface.

Some researchers have reported the application of the scratch test to ultrathin films. Recently, Covarel et al [58][59] investigated the feasibility of applying scratch testing to the adhesion and damage behaviour of sub-micron electronic polymer coatings on a 125 μm thick flexible semi-crystalline polymer substrate. The elastic, viscoelastic and plastic deformations caused 'pile-up' of the polymer film ahead of the scratch indenter (with a radius of 200 μm), which could be seen in the SEM micrographs and optical micrographs. They could not detect any sudden bursts of the signals from the plotted AE intensity against normal load curve and thus it was inferred that to find the critical load from acoustic emissions and micrographs was not feasible. However, when a scratch indenter with only a 5 μm tip radius was used, the delamination was induced at the position where the maximum 340 MPa shear stress is located 0.7 μm beneath the tip-coating contact. Subsequently, it was calculated that the scratch indenter with 200 μm tip radius resulted in the 280 MPa maximum shear stress, located about 23 μm beneath the tip-coating contact.

Many scratch tests are typically performed in ambient conditions. Such commercially available scratch testers such as the microscale Tribometer® or nanoscale Triboindenter®, are equipped with either a low or high temperature and humidity test chamber or a sample stage heater to conduct the scratch test at a temperature as high as 1000 ^{o}C. For example, Pujante et al [60] reported the results of scratching a hard physical vapour deposition (PVD) coating deposited on the surface of treated tool steel, at high temperatures up to 500 °C.

The outcomes from scratch tests are not only the adhesion strengths of coatings on substrates, but also the mechanical properties of the coatings, such as their tribological behaviour and corrosion resistance. Therefore, scratch tests have recently been employed for bilayer and multilayer hard, but ductile, metal and alloy coatings on ductile metal substrates, although micrographic morphology of scratch traces scarcely unveiled the cracks, delamination and other adhesion failures [61][62][63] that occurred.

Since most commercially available instruments can conduct both indentation and scratch tests, many researchers have deployed both micro- and nano-indentation and scratch testing in their experimental coating-substrate adhesion studies [64][65][66][67]. These sometimes are undertaken in test to compare adhesion properties, but more often for determining hardness and Young's modulus of elasticity.

Due to the high values of thickness and surface roughness of thermal spray ceramic coatings, scratch testing on the cross-section of coating-substrate systems has advantages over the standard scratch test method, shown in Fig.1. As a result of this, ISO/TC 107 recently has standardized scratch testing on cross-sections of thermal sprayed ceramic coatings [68]. Four years before the publication of that standard, Vencl et al [69] had evaluated the adhesion or cohesion bond strength by using the scratch testing of thick plasma spray coatings on cross-sections and the indenter was slid from substrate towards the coatings. In this work, the thickness of four coating-substrate samples was seen to vary from 270 μm to 400 μm. However, the scratch adhesion testing of the thermal spray ceramic coatings considered has not just been restricted to cross-section studies. Palanivelu and Kumar [70] conducted scratch testing of plasma spray nano-ceramic bilayers coated on titanium substrates in order experimentally to verify that a bilayer-coated medical grade titanium surface had an improved wear rate coefficient of friction, compared to monolayer coated surfaces (although in the work the bilayer coating thicknesses were not revealed).

The laser scratch or ablation method, just as the name implies, can be implemented by using pulsed light from an infrared Nd: YAG laser to characterize the interface bond strength, σ_B, by detecting the scratch damage using thermography [71][72][73]. The coating layer absorbing the laser energy is heated and diffuses the heat, so a temperature gradient is formed. Due to the differences in the thermal expansion and

the consequent temperature arising between the coating and substrate, a bending thermal stress, given by σ_{th}, is generated mainly in the normal direction of coating. It is expressed by

$$\sigma_{th} = \frac{M}{W_Z} = \frac{\alpha t E h^2}{12} \cdot \frac{6}{h^2} = \frac{\alpha t E}{2} \tag{4}$$

where M is bending moment in coating's rectangular cross-section area with thickness h and unit length b=1:$M = \alpha t E b h^2/12$ (unit: mm^4); W_Z is anti-bending cross-section modulus:$W_Z = bh^2/6$ (unit: mm^3); α is the thermal expansion coefficient of the coating, t is temperature difference of top-surface and bottom-surface of the coating; E is elastic modulus. If it rises to a certain value, where the original stress in the coating thickness direction is given by σ_z ,and the normal peel-off stress by $\sigma_S = \sigma_{th} + \sigma_Z$ (and this is larger than the interfacial bond strength σ_B), then with the stress beyond σ_B, cracks may appear. Thus, if the normal crack stress is σ_x, and the shearing force between coating and substrate is τ_{zx}, beyond that value, if the laser energy further increases, cracks will expand and spread and as a result, the coating will delaminate and peel off. The force diagram is shown schematically in Fig.*6*(a), with the experimental set-up used to create it shown in Fig.*6*(b). Considering equation (4), the peel-off stress σ_S is rewritten as

$$\sigma_S = \frac{\alpha t E}{2} + \sigma_Z \tag{5}$$

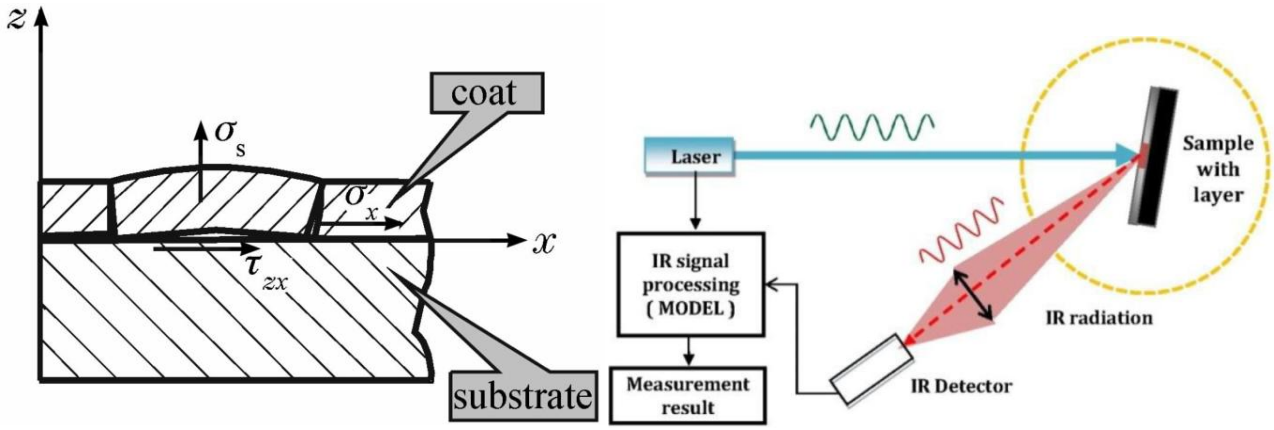

(a) (b)

Fig.6(a) Force diagram of coating peel-off after scratched by laser [71]; (b) Scheme of Nd-YAG pulse laser active and lock-in thermography for non-destructive testing [72].

The analysis of laser scratching of coatings was based on having a metal as a substrate and other non-metallic materials as a coating, to find the critical damage point of the coating position. The infrared laser first heats the coating and then gradually changes the temperature of the upper surface of the substrate through its thermal conductivity. Due to the difference in the absorbance of the laser power, the thermal expansion coefficient, the thermal conductivity and the heat sensitivity of the coating and the substrate, the relationship between the surface temperature and the laser power will change during the laser irradiation, as shown in Fig.7. There are two stages in the temperature change process. From Fig.7, it can be seen that in the section AB, the coating temperature rises most quickly, whereas in the section BC this effect saturates since the laser power has destroyed the coating and the laser irradiates the surface of the substrate. As the substrate metal material has a very low rate of absorption of the long wavelength of the laser, the temperature rises slowly. The turning point (shown as point B on Fig.7) of the temperature change is the critical position at which the coating begins to completely peel off the substrate. The corresponding laser power, P_o, is thus the minimum power required for the coating to peel off from the substrate and the corresponding critical temperature is given by T_o. Combining equation (5), Fig.6 (a) and Fig.7, we can modify the de-bonding stress σ_s, as

$$\sigma_S = \frac{\alpha E (T_B - T_A)}{2} + \sigma_Z \tag{6}$$

where, E is elastic modulus, α is the thermal expansion coefficient of the coating and T_A is initial temperature of the coating when laser scratching starts. However, it can be seen from Fig.*7* that the critical temperature point, B, is not so well defined and its position is open to judgement.

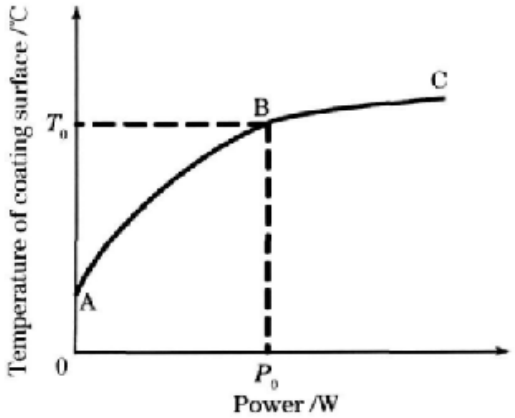

Fig.7 Schematic of the relationship between the temperature reached and the laser intensity impacting on the coating [74]

In contrast to the situation where a continuous scratch along one direction of a coated surface with increasing normal load exerted is created with a mechanical indenter, in the laser scratch test discrete scratching/ablating has been performed at different pre-set points along one direction on the coating surface. This is done by using the focused laser beam as a shock-scratching tool (with increasing power at different set-points), this being shown schematically in *Fig.8*, where, the points labelled 1, 2, 3 and 4 are the illustrated set-points with increasing laser power. It can thus be inferred that it may take time for the coating at these pre-set points to absorb enough laser energy to induce de-adhesion. When investigating the effects of laser ablation-induced coating removal, Shamsujjoha et al [75] proved that multiple laser passes were required to remove the epoxy-based coatings used.

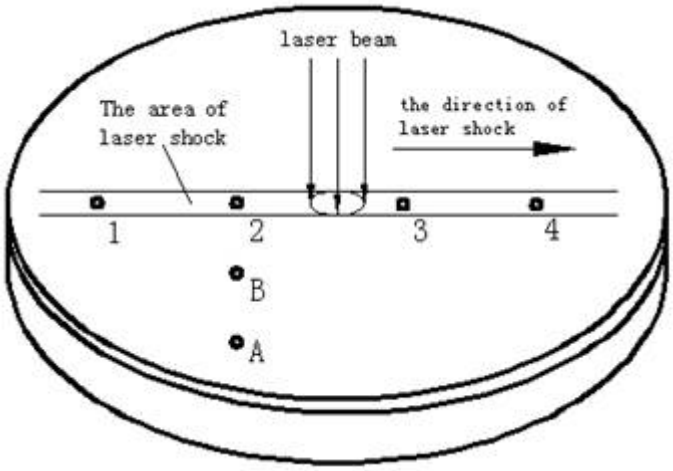

Fig.8 Schematic of laser scratch points and their positions [76]

However, the laser scratch test was shown to be effective not just for epoxy-based coatings on metal substrates, Yin et al [76] attempted to use a pulsed laser scratch test approach to study the adhesion of a TiN coating on steel substrates as this seemed to be a feasible method for this. The particular setup used in laser scratching was different from that used in the laser shockwave spallation method, in which the incident laser beam was focused onto the absorbing layer bounded on the substrate surface. The laser spallation adhesion test will be considered in Section 5 of this paper.

4. Blister, bulge and buckle testing

Blister, bulge and buckle tests are suitable to examine the interfacial adhesion of elastic or flexible coatings to plastic or rigid substrate systems. Jiang and Zhou et al [77][78] have updated the numerical modelling of a pressurised blister test. Blister testing can be used quantitatively to estimate the interfacial fracture toughness and adhesion. Pressurised blister testing has mainly been applied to thin coating systems, such as thin membrane films.

For blister and buckle testing, an external force (or pressure) is exerted through an inlet hole onto one surface of the test film, which then induces the blister, bulge and buckle phenomenon, as shown schematically in Fig.9. Given the recent extensive progress in the field of blister testing, a number of different types of blister tests have been categorised as follows: a) shaft loaded blister test, b) thermos-induced blister test, c) gas and liquid pressurised blister test, d) electrochemical reaction blister test, e) indentation and scratch induced blister test and f) the complicated blister test.

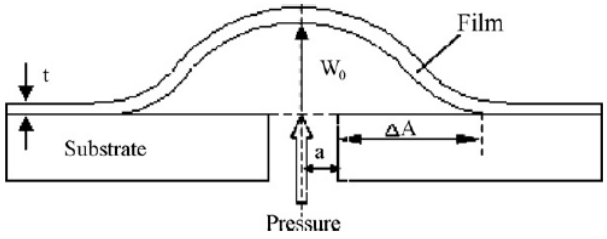

Fig.9 Schematic of the pressurized blister test: a through-hole of radius a, a circular blister with radius ΔA and height W_O [77][78].

4.1 Shaft loaded blister test

As shown in Fig.10, a shaft loaded blister test can be implemented, for example by using a spindle, a pillar or a ball [79][80]. In recent work, Islam and Tong [81] have experimentally investigated the relationship between the shaft diameter and the de-bonded blister radius, in order to establish their effects on the energy release rate for a metal-polymer composite coating system. Sun et al [82] developed a theoretical model for interfacial adhesion and the coating mechanical properties, such that Poisson's ratio and Young's modulus could be derived synchronously from the shaft-loaded blister test.

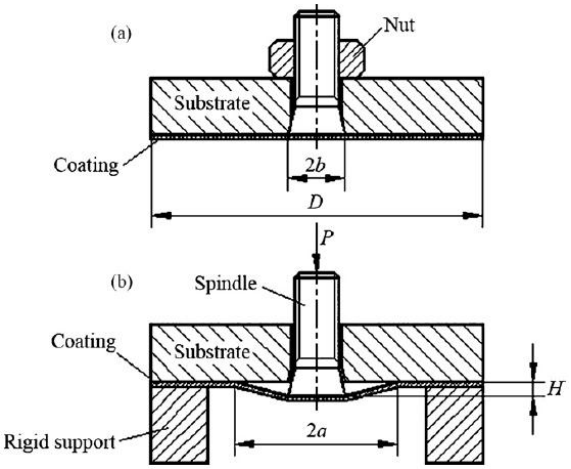

Fig.10 Schematic diagram of the setup of (a) a tested piece and (b) spindle cut through inducing blister [79]

4.2 Thermo-induced blister test

Guo et al [83] have tested circular blisters induced by annealing temperatures between 300°C and 500°C, to measure the brittle TiN film adhesion to brittle Si substrates coated with silicon dioxide at these high

temperatures. This annealing-induced blistering is actually a gas pressurised blistering effect. Galindo et al [84] implanted helium ions on the metal substrate before ceramic-coating, so that the expanding helium gas at the ceramic-metal interface induced blistering on heating. Wu *et al* [85] have made use of an alternating current generated thermodynamic impact load to investigate dynamic buckling of thin and flexible constantan film lines from polymer substrates. Under the thermodynamic impact load, the temperature of the film lines increases rapidly, which causes the film to expand and induce partial delamination from the substrate to form buckled blisters.

4.3 Liquid and gas pressurised blister test

The typical liquid and gas-pressurised blister test setup is shown in Fig.11 and Fig.12 respectively. During pressurized-blistering, the diameter of the blister and the liquid or gas pressure are monitored to calculate numerically the adhesion, according to the theoretical model given in the literature [86][87].

In practical terms, the blister can be induced by pressurised deionised water [86][87], oil [88] or compressed air [89]. Hailesilassie and Partl [90] have experimented with liquid generated blisters and their propagation under a 500mm x 500mm modified polymer bitumen membrane (PBM) on the similar-sized concrete plate.

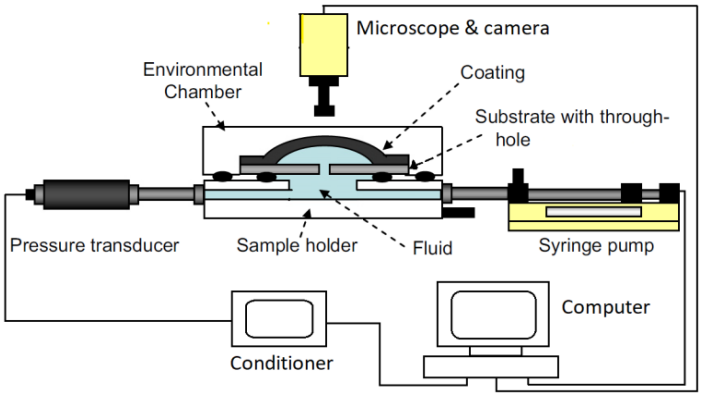

Fig.11Schematic of the liquid pressurized blister test apparatus which is modified from [86][87]

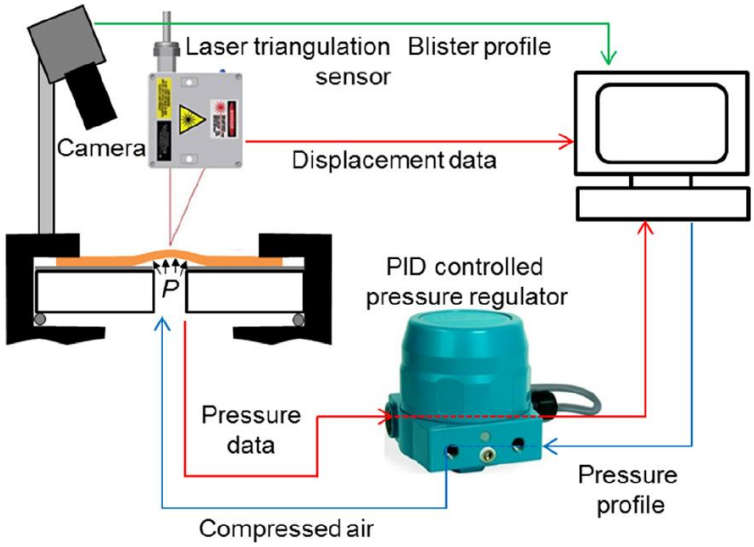

Fig.12 Schematic of the compressed air blister test setup [89]

4.4 Electrochemical reaction blister test

Corrosion-induced blistering has long been identified as a problem with polymer coatings on metal substrates. Electrochemical reaction blister testing is an accelerated means to simulate the aggressive environmental corrosion and erosion causing the adhesion loss of coating-substrate systems. Investigating corrosion-induced adhesion loss, Mills and Jamali [91] used sample immersion for the accelerated laboratory

testing of the coated metals, both in terms of intermittent and continuous immersion techniques. Schachinger et al [92] have experimented using osmotic- and cathodic-blistering on galvanized coatings on steel in oxidizing alkaline solutions and studied blister formation and growth by using electrochemical impedance spectroscopy (EIS). Souto et al [93][94] have characterized organic coating degradation and blistering on the metal substrate system induced by electrolytic immersion and using scanning electrochemical microscopy (SECM). The same SECM technique was employed to look at the issue of paint coating damage [95]. ISO has updated the standards on using electrochemical noise measurements [96], EIS [97][98][99][100][101] and cathodic polarization [101] to process, analyse and determine the mechanistic information generated in the breakdown of coatings. In addition, eddy current pulse thermography has also been investigated as another technique for the detection of corrosion blistering [102].

4.5 Compression-induced buckling blister or delamination

When a thin elastic film on a rigid substrate structure is subjected to a compressive stress, buckling occurs in the form of either blisters inside, or delamination from, the edge of the film. Hydrogen ion fluxes directed onto nanometre thick single-layers [103] or multilayer structured films [104][105] penetrate the films to the coating interfaces. The compressive stress, σ, in the film layers causes buckling blisters attributed to the over-pressurised hydrogen gas trapped in the delamination zones. The blister severity was found to be related to the intensity of hydrogen ion energy, with high energy ions resulting in more severe blistering.

When the compression load applied along the direction parallel to the film-substrate interface exceeds the critical strain, the buckling-induced bulges and delamination happen inside and from the edge of the film. In conducting compression-induced buckling delamination experiments, Zhu et al [106] applied FEM simulation and characterized the interfacial adhesion of a Ni thin film on a steel substrate; they developed contoured 3D plots of the evolution of the buckling morphologies under different compressive strains, ε, to find the critical buckling strain, where the interface defect initiates and the buckling bulge propagates. Consequently, they quantitatively analysed the process of buckling-induced delamination using analytical modelling, based on the energy minimization principle and numerical models based on FEM simulations. Wang et al [107] believed that a film-substrate system, when subjected to uniform compression, would generate a buckling delamination induced micro-channel, with a potential to direct and manipulate micro-fluids flowing through it. The study not only predicted the buckling delamination evolution but also characterised the buckling induced micro-channel. These investigators also analysed the relationship between micro flow and compressive strain.

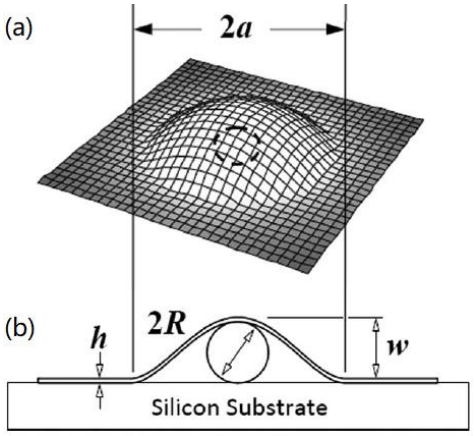

Fig.13 A typical circular blister traps a nanoparticle at the interface: (a) a 3D characterisation; (b) schematic of blister for modelling and analysing [111].

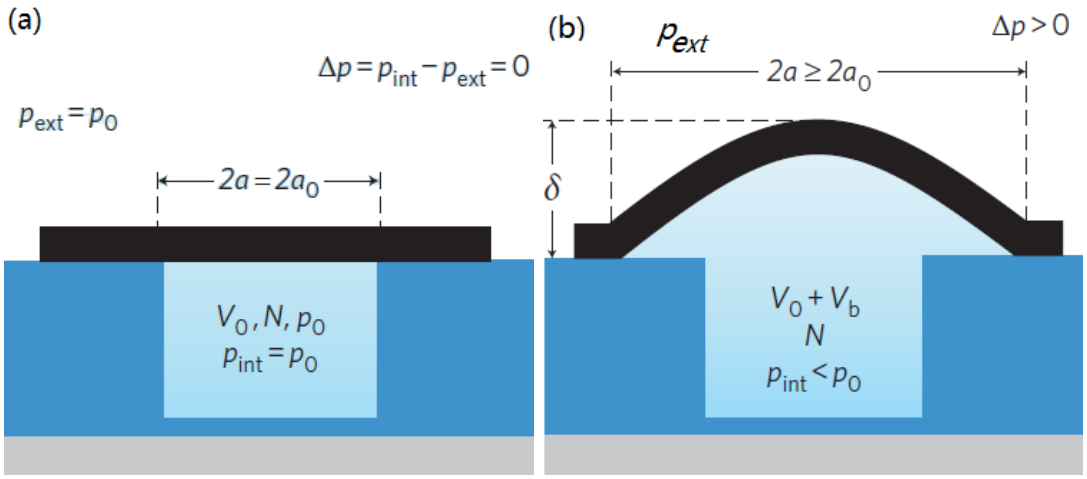

Fig.14 (a) Schematic pressure changes of a graphene-sealed micro-cavity in radius a_0: before it is inside the pressure chamber (PC) with pressure P_0, cavity inside pressure $P_{int}=P_{ext}$ (external pressure), so that the graphene membrane is flat; after about 5 days inside the PC Pint increased to P0. (b) After the micro-cavity is removed from the PC, $P_{int} < P_0$, which causes graphene to blister over the cavity and causes the blister radius ***a*** to increase [113].

Blister testing has been broadly applied to thin films of nanomaterials, especially for the fabrication and manufacture of large-area 2-dimensional graphene. Its surface adhesion to substrates and matrixes plays a very significant role when 2D graphene is integrated into MEMS devices and microelectronics, as well as composite materials. The surface adhesion has also a strong positive or negative influence on transferring the fabricated graphene onto or from the substrate [108]. Xin et al [109] have employed a similar liquid-pressurised blister test to gauge the adhesion energy of graphene, grown on a copper foil by the chemical vapour deposition (CVD) process. They have developed a method to create a through-hole in the copper foil, which can avoid damaging the graphene layer. Bunch and Dunn [110] have reviewed the adhesion mechanics of graphene membranes. They concluded that the graphene conformation to the silicon substrate is due to the strong influence of van der Waals forces, based on their theoretical analysis and experimental blister-testing. Additionally, Zong et al [111] have utilised the vacuum of a SEM chamber to measure graphene adhesion on silicon wafers. They deployed intercalated nanoparticles on the substrate surface to support the blisters, so on pump-down, the vacuum chamber causes the air trapped in the blister voids to expand. Based on the geometrical sketch of blisters shown in Fig.*13*, the measurement of adhesion energy was given by a theoretical equation model:

$$\gamma = \lambda E h \left(\frac{w}{a}\right)^4, \tag{7}$$

where, the geometrical factor λ=1/16, h is the film thickness, a and w are the blister radius and height respectively and E is the elastic modulus of the film. Using the same pressurised graphene blister mechanism, Li et al [112] fabricated an array of nano-pillars on the silicon substrate and then transferred the CVD graphene sheet onto the substrate, to produce an array of circular blisters. They used this novel blister approach to quantify the adhesion energy. Koenig et al [113] have designed and fabricated a pressurised blister test for the measurement of the adhesion energy of mechanically exfoliated graphene sheets on a silicon oxide substrate ion-etched with predefined wells. In a nitrogen gas pressure chamber, a few layers of graphene were conformed to the SiO_2 substrate and formed membranes over the wells sealing the micro-cavities, containing trapped nitrogen (N_2) gas molecules. After removal of the sample from the pressure chamber, the differential between the internal and external pressure of the cavities causes the membrane to blister over the cavities (as shown in Fig.*14*). An AFM was used to measure the 3D shape of the graphene membrane to find the deflection height, δ, and radius, a, of the blisters. In a similar way, Metten et al [114]

ion-etched cylindrical pits on a Si/SiO_2 substrate and deposited the mechanically exfoliated graphene over it to form the micro-cavities. In contrast, they used micro-Raman spectroscopy to determine the blister height, from the intensity of the Raman spectrum obtained, because the intensity of the Raman G- and 2D-mode features are very sensitive to the distance between the graphene membrane and the Si substrate.

In addition to these techniques, other well-known adhesion failure testing methods can also induce blisters, such as laser shock blasting, nano-indentation and nano-scratching. The adhesion of polymer coatings on metal substrates was previously studied using pulsed laser-induced blistering [115]. In this case, the blister shape and height were measured using a stylus profilometer in tandem with blister pressure measurements from a separate gas circuit set-up. A controlled, pulsed laser beam delivered pulses perpendicular to the polymer film, causing the metal substrate to absorb infrared radiation, which releases gas and initiates blister growth. Nano-scratch induced blistering [116] has usually been looked at with a micro- and nano-indentation tester, primarily for metal /non-metal (or *vice versa*) coating systems.

5. Pulse laser induced shock spallation

Pulse laser induced shock spallation can test the dynamic failure of coatings as a result of delamination, which is also termed laser spallation.

Laser induced spallation and shock testing is a mechanical stress-related de-adhesion process. Silicone grease or sodium silicate is injected on to the rear side of a substrate to form a confining layer. The substrate had previously been coated with a transparent thin layer of gold or aluminium, so a sandwich structure is created on that side and the metal coating can act as an energy absorbing layer, as shown in Fig.*15* (a) [117]. A laser pulse then impacts the absorbing layer, resulting in the generation of a strong and high amplitude acoustic pulse wave. The elastic wave propagates through the substrate thickness to the test coating which is on the other side of the substrate and is reflected at the free surface of coating. This leads to interference of the incident and the reflective wave, which then impacts on the interfacial stress. When the stress reaches the critical interfacial strength of the coating, delamination and spallation may happen, as shown in Fig.*15* (b). The parameters relating to this physical approach of the laser-absorbing layer/matter interaction, the shock wave propagation and the interface fracture were reviewed in [118][119].

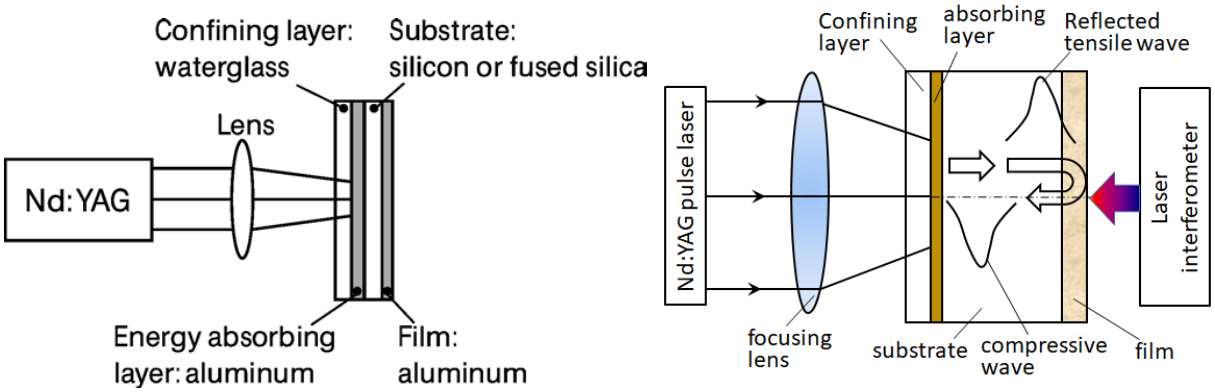

(a) (b)

Fig.15 Schematic setup of laser-induced spallation in (a) [117] and schematic principle of laser-induced film delamination in (b).

Laser spallation for interface toughness measurement methodology was proposed as early as 1990 by Gupta et al [120]. They applied the method for the adhesion determination of Si/SiC systems using a transparent fused quartz film as the confining layer and choosing a thin gold film as the energy absorber because of its optimum properties. Gold has a high melting temperature, large coefficient of thermal expansion and elastic

modulus, but a low thermal diffusivity, which means that it is very efficient in converting laser pulses into pressure pulses. The same group experimentally optimized the effect of the thickness and materials of the constraining and energy-absorbing films in terms of the strength of generated stress pulse. They reported that using a 0.5µm Al film as the energy absorbing film and a 5µm layer of solid sodium silicate as the constraining material was optimal. In 2008, they developed laser spallation to determine the tensile strength of cell and biomaterial interfaces [121].

The effect of delamination and spallation of coatings during adhesion testing reflects an out-of-plane-displacement velocity, which as a function of time was measured by a Doppler-principle based laser interferometer. When laser shock adhesion testing was exploited for ductile-ductile systems such as cold-sprayed Cu coating on Cu and Al substrates [122], the highest tensile stress that causes the interface de-adhesion could be morphologically observed from well prepared TEM cross-sections or metallography and X-ray diffraction [123]. The images captured were compared with the respective velocity profiles obtained when the coated samples underwent different powers of laser pulsing, so that the threshold laser power could be identified. Even more, Kingstedt and Lambros [124] have captured spallation area evolution and spallation front velocity over about 40ns duration using ultra-high speed photography. In a different study, a laser-induced surface acoustic wave device was utilized to detect the occurrence of de-adhesion and delamination of coatings on substrates left behind by laser spallation shockwave testing [125]. Schneider [126] started characterizing the thin films and material surfaces using acoustic wave detection technology. A schematic setup of the pulse laser-induced surface acoustic wave detection device is shown in Fig.*16*.

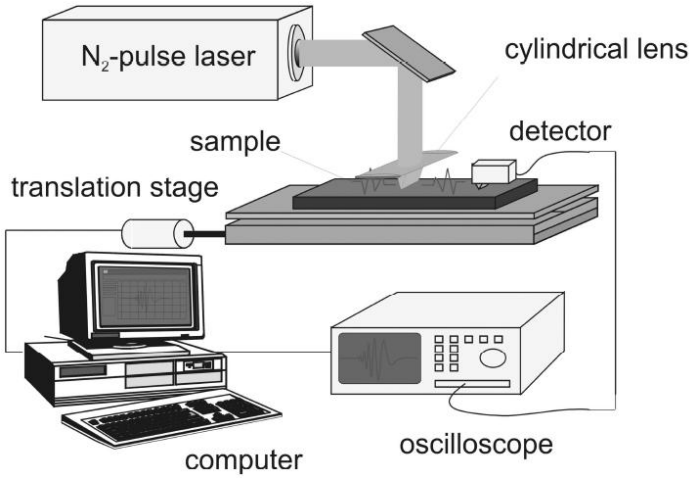

Fig.16 Schematic setup of the laser acoustic wave measuring systems [126]

To measure the out-of-plane-displacement velocity, a high frequency-response non-contact sensor, such as a high dynamic responding laser ultrasonic interferometer [127], is needed. The degree of damage and damage dimensions (i.e. fracture), including the minimum width of delamination radius can be measured from the scanned profiles. To convert the stress from the measured out-of-plane displacement, a one-dimensional wave equation is first employed [128]:

$$\sigma = \frac{1}{2}\rho C_L \frac{\partial u}{\partial t} \tag{8}$$

Where $\boldsymbol{\sigma}$ is the normal stress, $\boldsymbol{\rho}$ is the material density, $\boldsymbol{C_L}$ is the longitudinal wave velocity, and $\partial u/\partial t$is the velocity of out-of-plane displacement of the coating. Arai et al [129] have undertaken an experiment with a laser spallation setup similar to that reported in [127] and used a laser interferometer to measure the stress wave de-bonding displacement velocity using a Ti-coated film on an Al-alloy substrate. As part of this, they analysed the bond fracture toughness using a transfer function computed from the recorded displacement.

Based on the same debonding mechanism, laser spallation testing has been the subject of further developments. Perton et al [130], Ecault et al [131][132] and Gay et al [133] have applied laser induced shockwaves to study the damage and delamination of structured layers of carbon-epoxy and carbon fibre reinforced polymer (CFRP) composite ply respectively. More recently, the model for the laser-induced shock de-adhesion testing of the layered-composite materials has been numerically updated [134]. Rafieerad et al [135] have applied laser spallation to investigate the adhesion strength of a ZrO2-TiO_2-Nb_2O_5-Al_2O_3 mixed nanotube arrayed layer structure grown on Ti_6Al_7Nb alloy implants, by physical vapour deposition (PVD).

Courapied, Berthe, et al [136] have in their work improved the laser spallation test by developing a 752 nm Nd:YAG laser pulse-delayed double shock-wave generation apparatus, where the tested sample is immersed in water to act as the confining layer. This same technique has also been applied to evaluate the adhesion of thermal sprayed coatings on a textured surface [137].

All these techniques discussed have used the pulse laser induced tensile spallation test shown in Fig.*15* and the interface failure of the coating and the substrate is caused by the tensile stress. Wang et al [138] and Kitey et al [139] modified the tensile spallation testing by sandwiching a fused silica disk between the energy-absorbing layer and the substrate, as shown in Fig.*17*(a). They further improved the set-up by incorporating the fused silica in the form of a triangular prism so that the tensile spallation test evolved into a tensile and shear mixed-mode spallation test, as shown in Fig.*17* (b). In this case, the interface failure between the coating and the substrate is caused by the tensile and shear stresses.

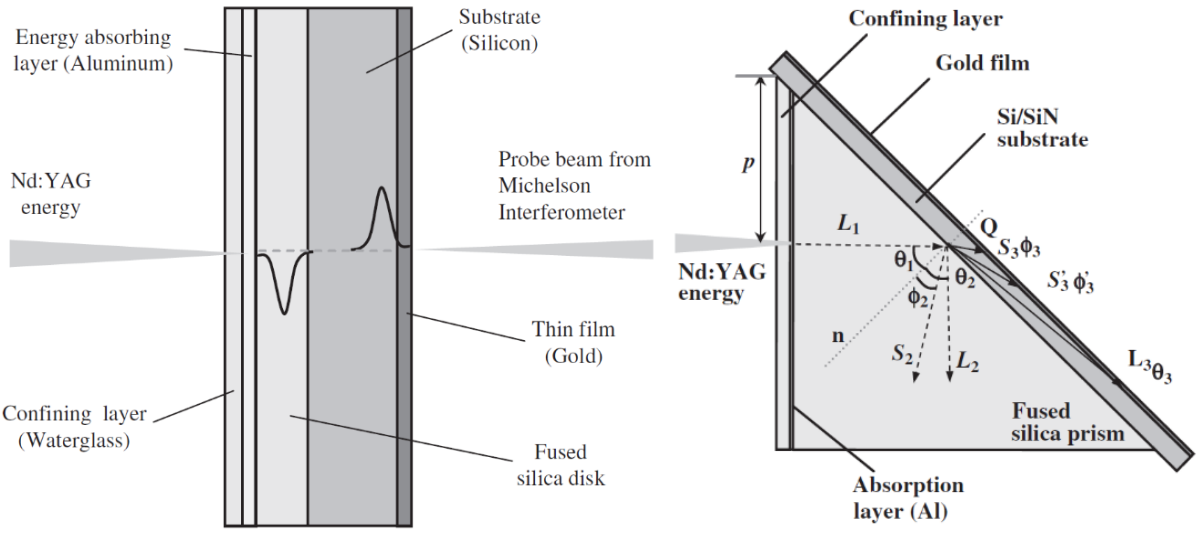

Fig.17 Schematic of (a) laser tensile spallation and (b) mixed-mode spallation specimen geometry [139]

Further work on laser tensile spallation testing by Tran et al of the UIUC [140] compared dynamic laser tensile spallation testing and quasi-static four-point bend testing on the adhesion of an Al thin film on a Si substrate.

Aiming at the future practical application of the laser shock spallation adhesion test (LASAT) directly on ceramic TBS-coated metallic turbine blades, Bégué et al [141] qualitatively approached the LASAT by directing the laser radiation not only from the metallic side (MS) but also from the ceramic coating side (CS). The interfacial cracks that resulted from both the MS and CS tests were observed as white spots appearing in the optical images taken from the ceramic side. The relationship between the spot diameter and the real interfacial crack size was established for both the MS and CE tests by experimentally examining the cross-sections under the SEM and from lifetime-decay maps of photoluminescence measured by piezospectroscopy. In order to study further the shear loading influence on the growth of interfacial white areas initiated by the laser shockwave spallation, Sapardanis et al [142] applied biaxial loadings (compression

loading in one axis and tension loading in another axis) to cruciform shaped metallic substrates with alumina coatings in the centre deposited by plasma spray with 28mm diameter areas. It was observed that the initial interfacial circular crack blistering near the centre, induced by laser shockwave spallation MS testing, grew to quasi-elliptical forms with semi-major axes(a) in the tension direction and semi-minor axes and (b) in the compression direction. The ellipse ruptured along the biaxial loading directions.

In an alternative setup to induce laser shockwave damage, the laser irradiation has been configured from the inside of the crystal film interface layer [143].

The phenomenon observed that laser pulsed shockwave spallation induces thin film de-bonding and local rupturing has also been exploited for the nanofabrication of microstructures. As an example, a pattern of micro square, circular and star-shaped holes was created in an Au-film coated on polyimide and K9 glass substrates, as shown in Fig.*18*, using a micro-mould with similar shaped holes [144] (i.e. similar to a photo-mask technique in the optical lithography).

The testing of coating adhesion on a super-hard aluminium substrate can be fulfilled by employing pressurised blister and AFM scratch methods for one coating material [145] or by using laser spallation, bulge and blister testing for another coating material [146].

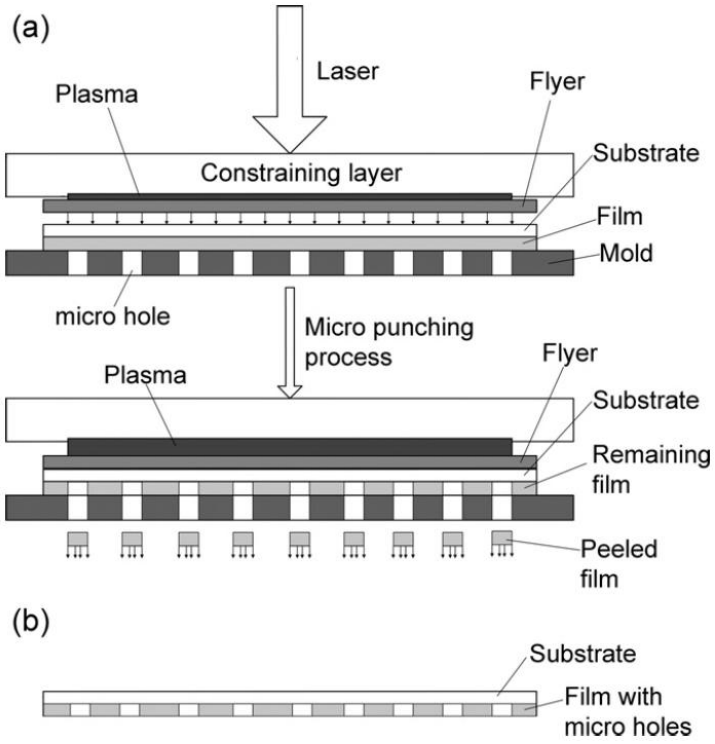

Fig.18 Schematic of spallation de-bonding induced by laser driven-flyer (absorbing layer) shockwave for micro-punching process in (a) and the punched a pattern of micro holes on the film in (b) [144].

6. Other adhesion tests induced acoustic emission and measurements

Measuring the acoustic emission requires the detection of an elastic wave which is generated when the micro-scale defects instantaneously occur [147].For coating-substrate systems, the coating or substrate micro-scale defects and failures are induced by several different mechanical testing methods.

As an established NDT monitoring technique in mechanical and materials research for detection of plastic deformation, fracture initiation and crack growth, acoustic emission refers to the generation of transient elastic waves produced by a sudden redistribution of stress in a material. When a coating-substrate system is subjected to an external stimulus, such as the change in pressure load or temperature, localized sources

trigger the release of energy in the form of stress waves. The stress waves propagated to the surface or interface of coatings and substrates and were recorded by different sensors [148][149]. Using the right sensors and detection instruments, displacements of the order of picometres (10^{-12} m) can be detected. Interesting AE sources result from the initiation and growth of cracks, slips and dislocation movements, as well as melting, twinning, and phase transformations in metals. Matrix cracking, fibre breakage and debonding in composites also contribute to acoustic emissions [150]. Acoustic emissions have also been measured and recorded in polymers, wood and concrete, among other materials.

Formerly acoustic emission was regularly applied to the detection of leaks in valves, pipeline, sewers and tanks, and the detection of corrosion and stress corrosion cracking in plant equipment. Since 2010, numerous investigations into various aspects of coating technologies [151][152][153][154][155][156], including corrosion and fluid immersion processes have been undertaken.

Yang et al [157] have measured and evaluated the acoustic emission of fracture in thermal barrier coatings by using bending testing methods. A tensile test coupled with AE detection and combined digital image correlation [158] was carried out especially in thermal barrier spray coatings. During thermal cycle test of the fracture behaviour of ceramic coating, the AE signal was analysed and measured by using laser interferometry [159][160]. Lowers, Yoshida, et al [161][162] have applied low frequency acoustic waves to agitate the thin film system from the real surface of the substrate. As the acoustic wave magnitude is insufficiently high to excite an acoustic wave in the rigid substrate but high enough to stimulate the harmonic motion in the coating-substrate interface with lower stiffness than the thin film or substrate, the displacement of the thin film is considerably larger than that of the substrate and subsequently the de-adhesion of thin film coating happens. The displacement was measured by use of a Michelson interferometer.

The advantage of AE testing is that it is often performed on structures whilst they are in operation, as this provides adequate loading for propagating defects and triggering acoustic emissions.

In summary, the disadvantages of AE testing are:

a) AE testing systems can only qualitatively measure how much damage is contained in a structure. To obtain quantitative results about other key parameters such as size, depth, and overall mechanical properties such as coating bond strength/adhesion to the substrate, other NDT methods (e.g. ultrasound detection [163]), modelling and model-based calculation analysis [164] are necessary.
b) Other acoustic emissions also originate in the noisy service environments in which the AE testing is taking place, which contributes extraneous noise to the signals. For successful applications, the application of signal discrimination and noise reduction methods is crucial [165][166].

7 Option of adhesion testing methods and discussion

The coating-substrate systems are catalogued as ductile-ductile (D-D), brittle-ductile (B-D), ductile-brittle (D-B), brittle-brittle (B-B) systems. The classification is based on the ability of a material to experience plastic deformation. Ductile materials exhibit substantial plastic deformation with high energy absorption before fracture, whilst brittle materials have little or no plastic deformation with low energy absorption [167]. For ductile materials, extensive plastic deformation resists any further extension of a crack unless there is an increase in the applied stress, however, for brittle material, the cracks may spread extreme-rapidly without increase of applied stress. Many researchers, especially Guo et al [168] and Zhang et al [169], have focused their research into adhesion strength and interfacial toughness of a coating-substrate system, in terms of their 'brittle' and 'ductile' nature. Therefore, from the published literature we have reviewed in this paper, we summarise the applicability of indentation, scratch, blister and laser spallation testing to the adhesion of coherently catalogued coating-substrate systems. This is shown in table 1, where indentation 1, 2 and 3 denote on-coating surface indentation, cross-sectional indentation and interfacial indentation, respectively.

Table 1 The applicability of testing methods to the coating-substrate system

	Thin-coatings (<20 μm)				Thick-coatings (≥20μm)			
	D-B	D-D	B-B	B-D	D-B	D-D	B-B	B-D
Indentation 1	√		√	√				
Indentation 2					√		√	√
Indentation 3					√		√	√
Scratch (by stylus)	√		√	√				
Scratch (by laser)					√		√	√
Blister	√	√			√	√	√	
Laser spallation	√	√			√	√		

Due to the differences in mechanical and thermal properties between the coating material and substrate material, under the various mechanical and thermal loads implemented by indentation, scratch, blister and laser spallation, the mismatch between the stress and strain of the two materials leads to coating failures. Therefore, it is not demanding to use those adhesion testing methods to cope with a coating-substrate system with different mechanical and thermal properties. We can also briefly summarise the following:

(1) Indentation and scratch methods have the widest applicability among them, for either thin or thick coatings, although for on-coating surface indentation and scratch by stylus, these are the two most effective and applicable methods for adhesion testing of thin coatings;
(2) To use a blister method, although it is difficult to prepare the testing specimens for the ductile thin-film to have performed buckles and blisters prior to the testing itself, it is the most effective method to test the adhesion of 2D nanomaterial thin-coating-substrate systems;
(3) To use the laser spallation method, it is limited by the expensive pulse laser and velocity laser interferometer and it is difficult to build the theoretical modelling. However, it seems a most promising method for testing the adhesion of ductile coatings on ductile substrates.

Conclusion

The above review has discussed a number of techniques and approaches used in the field and shown the range of advances in testing and measurements on the interface adhesion and bond strengths in coating-substrate systems. The analysis of the published material has shown that coatings must exhibit sufficient adhesion to the coated substrates so that they provide the desired practical benefits when put into service. Importantly, the work reported has demonstrated that no single adhesion test is sufficiently versatile or universally applicable to every coating-substrate system. In many cases, a number of different adhesion tests may be required to fully satisfy the need for an adequate analysis of the coating. It is also worth noting that for some of the testing techniques, specifically prepared coating-substrate arrangements need to be created for the test, which may not match the way the coating is prepared in practice. Clearly in such cases, it is important to know that the same degree of adhesion can be achieved by the two coating arrangements.

Acknowledgement

We thank the research Executive Agency (REA), European Commission for the support to the InnoSMART project (Ref. 664892).

References

[1]. J Graystone, R Kennedy. Non-destructive measurement of coating adhesion, Surface Coatings International 83(2000) 389-398.DOI: 10.1007/BF02692753

[2]. A A Volinsky, N R Moody and W W Gerberich. Interfacial toughness measurements for thin films on substrates, Acta Materialia 50 (2002) 441-466. doi: /10.1016/S1359-6454(01)00354-8

[3]. J Chen, S J Bull. Approaches to investigate delamination and interfacial toughness in coated systems: An overview, J. Phys. D: Appl. Phys. 44 (2011) 34001 (14pp).doi:10.1088/0022-3727/44/3/034001

[4]. ISO 14577-1. Metallic materials - Instrumented indentation test of hardness and materials parameters - Part1: Test method (2015).doi:10.3403/30248588U

[5]. ISO 14577-4. Metallic materials - Instrumented indentation test of hardness and materials parameters – Part4: Test method for metallic and non-metallic coatings (2007).doi:10.3403/30268152U

[6]. B Ramamoorthy, B C Yeldose. An Investigation into the adhesion strength of diamond like carbon multilayer coating (DLC/TiN/Ti/Cu/Ni). Intelligent Information Management 1 (2009) 179-194. doi:10.4236/iim.2009.13027

[7]. A J Haq, P R Munroe, M Hoffman, P J Martin and A Bendavid. Berkovich indentation of diamond-like carbon coatings on silicon substrates, Journal of Materials Research 23 (2008) 1862-1869. doi:10.1557/JMR.2008.0232

[8]. F Hasan, J Wang and Ch Berndt. Determination of the mechanical properties of plasma-sprayed hydroxyapatite coating using the knoop indentation technique, Journal of Thermal Spray Technology 24 (2015) 865-877. doi: 10.1007/s11666-015-0228-0

[9]. A Sivitski, A Gregor, M Saarna, P Kulu and F Srgejev. Application of the indentation method for cracking resistance evaluation of hard coatings on tool steels, Estonian J. Eng 15 (2009) 309-317. doi:10.1016/j.engfailanal.2011.02.011

[10]. Y Yamazaki, M Suzuki, M Arai, Y Miyashita. Current activities for standardization on indentation method to evaluate adhesion strength of thermal spray coatings in Japan, Proceeding on International Thermal Spray Conference and Exposition, 2013.

[11]. Y Yamazaki, M Arai, Y Miyashita, H Waki, M Suzuki. Determination of interfacial fracture toughness of thermal spray coatings by indentation, Journal of Thermal Spray Technology 22 (2013) 1358-1365. doi: 10.1007/s11666-013-9961-4

[12]. ISO 19207:2016(E) Thermal spraying - Classification method of adhesive strength by indentation, 2016.

[13]. ISO 20267:2017(E) Thermal spraying - Determination of interfacial toughness of ceramic coating by indentation, 2017.

[14]. A Roshanghias, G Khatibi, R Pelzer, J Steinbrennerand J Bernardi. Cross-sectional nanoindentation (CSN) studies on the effect of thickness on adhesion strength of thin films. J. Phys. D: Appl. Phys. 48 (2015) 03301. doi:10.1088/0022-3727/48/3/035301

[15]. J Kim, J Jeong,K Lee, D Kwon. A new indentation cracking method for evaluating interfacial adhesion energy of hard films, Thin Solid Films 441 (2003) 172-179. doi:10.1016/S0040-6090(03)00920-9

[16]. G Lee, S Kang, D Kwon. Characterization of elastic modulus and work of adhesion in elastomeric polymers using microinstrumented indentation technique, Materials Science & Engineering A 496 (2008) 494-500. doi:10.1016/j.msea.2008.06.010

[17]. N K Fukumasu, R M Souza. Numerical evaluation of cohesive and adhesive failure modes during the indentation of coated systems with compliant substrates, Surface & Coatings technology 260 (2014) 266-271. doi:10.1016/j.surfcoat.2014.07.093

[18]. Y Xiao, W Shi, J Luo. Indentation for evaluating cracking and delamination of thin coatings using finite element analysis, Vacuum 122 (2015) 17-30.doi:10.1016/j.vacuum.2015.09.003

[19]. J Liu, X Wang, H Li,W Yang. Delamination mechanism maps for coatings/substrates system subjected to adhesive contact loads, Thin Solid Films 626 (2017) 159-167. doi: 10.1016/j.tsf.2017.02.042

[20]. J Chen. Indentation-based methods to assess fracture toughness for thin coatings, J. Phys. D: Appl. Phys. 45 (2012) 203001 (14pp). doi:10.1088/0022-3727/45/20/203001

[21]. ISO 26443. Fine ceramics (advanced ceramics, advanced technical ceramics)-Rockwell indentation test for evaluation of adhesion of ceramic coatings (2016).

[22]. X Fan, D Diao. The adhesion behavior of carbon coating studied by re-indentation during in situ TEM nanoindentation, Applied Surface Science 362 (2016) 49–55. doi:10.1016/j.apsusc.2015.11.196

[23]. P Wieciński, J Smolik, H Garbacz, K J Kurzydłowski. Failure and deformation mechanisms during indentation in nanostructured Cr/CrN multilayer coatings, Surface & Coatings Technology 240 (2014) 23-31. doi:10.1016/j.surfcoat.2013.12.006

[24]. M Trueba, D Gonzalez, J M Martínez-Esnaola, M T Hernandez, D Pantuso, H Li, M R Elizalde, I Ocaňa. Fracture characterization of thin-films by dual tip indentation, Acta Materialia 71 (2014) 44-55. doi:10.1016/j.actamat.2014.03.011

[25]. O Shikimake, A Burlacu, D Grabco, V Parvan, C Pyrtsacand V Ursaki. Mechanical properties and Raman scattering investigation under indentation of $CdGa_2S_4$ and $CdGa_2Se_4$, J. Phys. D: Appl. Phys. 49 (2016) 205302 (10pp). doi:10.1088/0022-3727/49/20/205302

[26]. A E Dolinko, G H Kaufmann. Measurement of the local displacement field generated by a microindentation using digital speckle pattern interferometry and its application to investigate coating adhesion, Optics and Lasers in Engineering 47 (2009) 527-531.doi:10.1016/j.optlaseng.2008.10.012

[27]. L P Tendela, G H Kaufmann. Evaluation of coating adhesion using a radial speckle interferometer combined with a micro-indentation test, Optics and Lasers in Engineering 50 (2012) 817–822. doi:10.1016/j.optlaseng.2012.02.004

[28]. P Poza, C J Múnez, MA Garrido-Maneiro, S Vezzù, S Rech, A Trentin. Mechanical properties of Inconel 625 cold-prayed coatings after laser remelting. Depth sensing indentation analysis, Surface & Coatings Technology 243 (2014) 51–57. doi:10.1016/j.surfcoat.2012.03.018

[29]. A Yeo, M Liu and K Zhou. Indentation damage evaluation on metal-coated thin-films stacked structure, J. Mater. Res. 30 (2015) 3071-3083. doi: 10.1557/jmr.2015.278

[30]. A Yeo, Y Kai, *et al*. Study on damage and fracture of thin-film stacked structures through indentation test with acoustic emission sensing, Intern. J. Mech. Sci. 128-129 (2017) 159-167. doi:10.1557/jmr.2015.278

[31]. G Marot, Ph Demarecaux, J Lesage, M Hadad, St Siegmann, M H Staia. The interfacial indentation test to determine adhesion and residual stresses in NiCr VPS coating. Surface & Coatings Technology 202 (2008) 4411-4416. doi:10.1016/j.surfcoat.2008.04.018

[32]. S Wen, X Zeng, and G Xie. Investigation on the interface characteristics of the thermal barrier coating system through flat cylindrical indenters, Adv. Mech. Eng. (2014) 654096 (10pp). doi: 10.1155/2014/654096

[33]. G Song, Zh Luo, F Li, L Chen and Ch He. Microstructure and indentation toughness of Cr/CrN multilayer coatings by arc ion plating, Trans. Nonferrous Met. Soc. China 25(2015) 811−816. doi: 10.1016/S1003-6326(15)63667-6

[34]. G Bolelli, B Bonferroni, H Koivuluoto, L Lusvarghi, P Vuoristo. Depth-sensing indentation for assessing the mechanical properties of cold-sprayed Ta, Surface & Coatings Technology 205 (2010) 2209-2217. doi:10.1016/j.surfcoat.2010.08.146

[35]. H Zhao, Y Zhong, Zh Ma. Effects of indentation depth on micro hardness and scratch behaviour of thin composite laminate. Journal of Alloys and Compounds 680 (2016) 105-108. doi:10.1016/j.jallcom.2016.04.108

[36]. S t Choi, S R Lee and Y Y Earmme. Measurement of time-dependent adhesion between a polymer film and a flat indenter tip, J. Phys. D: Appl. Phys. 41 (2008) 074023 (10pp).doi:10.1088/0022-3727/41/7/074023

[37]. M Annamalai, S Mathew, MJamali, D ZhanandMPalaniapan. Effects of annealing on the ripple texture and mechanical properties of suspended bilayer graphene, J. Phys. D: Appl. Phys. 46 (2013) 145302. doi:10.1088/0022-3727/46/14/145302

[38]. J W Suk, S R Na, R J Stromberg, D Stauffer, J Lee, R S Ruoff, K M Liechti. Probing the adhesion interactions of graphene on silicon oxide by nanoindentation, Carbon 103 (2016) 63-72. doi:10.1016/j.carbon.2016.02.079

[39]. P Li, Zh You, T Cui. Adhesion energy of few layer graphene characterized by atomic force microscope, Sensors, and actuators A 217 (2014) 56-61. doi:10.1016/j.sna.2014.06.010

[40]. Y Ding, P Zhang, H Ren, Q Zhuo, Zh Yang X Jiang, Y Jiang. Surface adhesion properties of graphene and graphene oxide studies by colloid-probe atomic force microscopy, Applied Surface Science 258 (2011) 1077-1081. doi: /10.1016/j.apsusc.2011.09.005

[41]. T Jiang, Y Zhu. Measuring graphene adhesion using atomic force microscopy with a microsphere tip, Nanoscale 7 (2015) 10760. doi: 10.1039/c5nr02480c

[42]. Sh Deng, A V Sument, V Berry. Strain engineering in two-dimentional nanomaterials beyond grapheme, Nano Today 22 (2018) 14-35. doi:10.1016/j.nantod.2018.07.001

[43]. J Chen, S J Bull. Multi-cycling nanoindentation study on thin optical coatings on glass, J. Phys. D: Appl. Phys. 41 (2008) 074009 (9pp). doi:10.1088/0022-3727/41/7/074009

[44]. L S Qiu, X D Zhu, S Lu, G Y He, K W Xu. Quantitative evaluation of bonding strength for hard coatings by interfacial fatigue strength under cyclic indentation, Surface & Coatings Technology 315 (2017) 303-313. doi:10.1016/j.surfcoat.2017.02.045

[45]. T Sander, S Tremmel, S Wartzack. A modified scratch test for the mechanical characterization of scratch resistance and adhesion of thin hard coatings on soft substrates, Surface & Coatings Technology 206 (2011) 1873-1878. doi:10.1016/j.surfcoat.2011.08.035

[46]. EN 1071-3. Advanced technical ceramics-Methods of test for ceramic coatings-Part 3: Determination of adhesion and other mechanical failure modes by a scratch test, 2005.

[47]. S.J. Bull*, E.G. Berasetegui. An overview of the potential of quantitative coating adhesion measurement by scratch testing, Tribology International 39 (2006) 99–114. doi:10.1016/j.triboint.2005.04.013

[48]. K Holmberg, A Laukkanen, H Ronkainen, K Wallin, S Varjus. A model for stresses, crack generation and fracture toughness calculation in scratched TiN-coated steel surfaces, Wear 254 (2003) 278–291. doi:10.1016/S0043-1648(02)00297-1

[49]. A Chatterjee, A A Polycarpou, e J R. Abelson, P Bellon. Nanoscratch study of hard HfB2 thin films using experimental and finite element techniques, Wear 268 (2010) 677-685. doi:10.1016/j.wear.2009.11.001

[50]. W Zhou, Y He, X LU. Acoustic emission in scratch processes of metals, insight: Non-Destruct. Test. Condition Monit. 57 (2015) 635-642.doi: 10.1784/insi.2015.57.11.635

[51]. R K Choudhary, P Mishra. Use of acoustic emission during scratch testing for understanding adhesion behaviour of aluminium nitride coatings, J. Mater. Eng. Perform. 25 (2016) 2454-2461. doi: 10.1007/s11665-016-2073-9

[52]. O Stankevych, V Skalsky, Investigation and identification of fracture types of structural materials by means of acoustic emission analysis, Engineering Fracture Mechanics 164 (2016) 24–34. doi:10.1016/j.engfracmech.2016.08.005

[53]. K Singh, N Krishnamurthy, A K Suri. Adhesion and wear studies of magnetron sputtered NbN films, Tribology International 50 (2012) 15-25. doi:10.1016/j.triboint.2011.12.023

[54]. A Gallego, J F Gil, E Castro, R Piotrkowski. Identification of coating damage processes in corroded galvanized steel by acoustic emission wavelet analysis, Surface & Coatings Technology 201 (2007) 4743–4756. doi:10.1016/j.surfcoat.2006.10.018

[55]. M A Hassan, A R Bushroa, R Mahmoodian. Identification of critical load for scratch adhesion strength of nitride-based thin film using wavelet analysis and a proposed analytical model, Surface & coatings Technology 277 (2015) 216-221. doi:1 0.1016/j.surfcoat.2015.07.061

[56]. X Cai, Y Xu, N Zhao, L Zhong, Z Zhao, J Wang. Investigation of the adhesion strength and deformation behaviour of in situ fabricated NbC coatings by scratch testing, Surface & Coatings Technology 299 (2016) 135–142.Doi:10.1016/j.surfcoat.2016.05.004

[57]. M. Zawischa, S. Makowski, N Schwarzer, V Weihnacht. Scratch resistance of super hard carbon coatings-A new approach to failure and adhesion evaluation, Surface & Coatings Technology 308 (2016) 341–348. doi:10.1016/j.surfcoat.2016.07.109

[58]. G Covarel, B Bendaid, X Boddaert, S Giljean, P Benaben, P Louis. Characterization of organic ultra-thin film adhesion on flexible substrate using scratch test technique, Surface & coatings Technology 211 (2012) 138-142. doi:10.1016/j.surfcoat.2011.09.057

[59]. X Boddaert, G Covarel, B Bensaid, M Mattei, P Benaben, J Bois. Organic ultrathin film adhesion on compliant substrate using scratch test technique, Thin Solid Films 528 (2013) 194-198. doi:10.1016/j.tsf.2012.07.138

[60]. J Pujante, M Vilaseca, D Casellas, M D Riera. High temperature scratch testing of hard PVD coating deposited on surface treated tool steel, Surface & Coatings Technology 254 (2014) 352-357.D\doi:10.1016/j.surfcoat.2014.06.040

[61]. C L Jiang, H L Zhu, K S Shin, Y B Tang. Influence of titanium interlayer thickness distribution on mechanical properties of Ti/TiN multilayer coating, Thin Solid Films 632 (2017) 97-105. doi:10.1016/j.tsf.2017.04.026

[62]. M S Kabir, P Munroe, PMunroe, ZhZhou, ZXie. Scratch adhesion and tribological behaviour of graded Cr/CrN/CrTiN coatings synthesized by closed –field unbalanced magnetron sputtering, Wear 380-381 (2017) 163-175. doi:1 0.1016/j.wear.2017.03.020

[63]. CH Chang, J Duh. Duplex coating techniques to improve the adhesion and tribological properties of CrAlSiN nanocomposite coating, Surface & coatings Technology 326 (2017) 375-381. doi:10.1016/j.surfcoat.2016.11.032

[64]. T Abubakar, M Rahman, D P. Dowling, J Stokes and M S. J. Hashmi. Adhesion performance of TiN Coating with amorphous NiTi alloy interlayer onto 316L stainless biosteel deposited by sputtering process, Surf. Eng. 26 (2010) 499-505. doi: 10.1179/174329409X433885

[65]. S Msolli, J Alexis, HS. Kim, O Dalverny, M Karama. Assessment of candidate metallization systems deposited on diamond using nano-indentation and nano-scratching tests, Thin Solid Films 619 (2016) 53-60. doi:10.1016/j.tsf.2016.10.022

[66]. H M S Iqbal, S Bhowmik, R Benedictus. Performance evaluation of polybenzimidazole coating for aerospace application, Progress in Organic coatings 105 (2017) 190-199. doi:10.1016/j.porgcoat.2017.01.005

[67]. S Das, D Lahiri, D Lee, A Agarwal, W Choi. Measurement of the adhesion energy of graphene to metallic substrates, Carbon 59 (2013) 121-129. doi:10.1016/j.carbon.2013.02.063

[68]. ISO 27307:2015. Thermal spraying – Evaluation of adhesion/cohesion of thermal sprayed ceramic coatings by transverse scratch testing, 2015.

[69]. A Vencl, S Arostegui, GFavaro, FZivic, MMrdak, S Mitrović, VPopovic. Evaluation of adhesion/cohesion bond strength of the thick plasma spray coatings by scratch testing on coatings cross-section, Tribology International 44 (2011) 1281–1288. doi:10.1016/j.triboint.2011.04.002

[70]. R Palanivelu, A R Kumar. Scratch and wear behaviour of plasma sprayed nano ceramics bilayer Al2O3-12wt%TiO2/Hydroxyapatite coated on medical grade titanium substrates in SBF environment, Applied Surface Science 315 (2014) 372-279. doi:10.1016/j.apsusc.2014.07.167

[71]. S Yin, Y Ye, A Feng, Ch Cheng. Theoretical analysis and testing research of stress-strain of coating scratched by infrared laser, Chinese Journal of Lasers 35 (2008) 1423-1428. doi:10.3788/CJL20083509.1423

[72]. A Semerok, C Grisolia,S V Fomichev, P-Y Thro. Laser active thermography for non-destructive testing, Proc. SPIE 9065 (2013) 90650A. doi: 10.1117/12.2053120

[73]. Y Cao, A Feng, Ch Xu, H Sun. Device of the laser discrete scratching for test interfacial bonding strength based on optimization algorithm, Chinese Journal of Lasers 37 (2010) 2160-2164. doi:10.3788/CJL20103708.2160

[74]. A Feng, Y Ye, S Yin, Ch Cheng and Y Cao. Theoretical analysis and experimental research on the broken critical-position of coating interface, Chinese Journal of Laser 35 (2008) 1746-1751. doi:10 .3788/CJL20083511.1746

[75]. Me Shamsujjoha, S R Agnew, M A Melia, J R. Brooks, T J. Tyler, J M. Fitz-Gerald. Effects of laser ablation coating removal (LACR) on a steel substrate: Part 1: Surface profile, microstructure, hardness, and adhesion, Surface & Coatings Technology 281 (2015) 193-205.doi:10.1016/j.surfcoat.2015.01.071

[76]. S Yin, Y Ye, A Feng, Y Cao. Experimental study on non-bounding layer TiN coating by pulsed-laser shock scratching, Chinese Journal of Lasers 37 (2010) 316-320.doi :10.3788/CJL20103701.0316

[77]. L M Jiang, Y C Zhou, Y G Liao, C Q sun. A pressurized blister test model for the interface adhesion of dissimilar elastic-plastic materials, Materials Science & Engineering A 487 (2008) 228-234. doi:10.1016/j.msea.2007.10.014

[78]. L Jiang, Y Zhou, H Hao, Y Liao, Ch Lu. Characterization of the interface adhesion of elastic-plastic thin film/rigid substrate systems using a pressurized blister test numerical model, Mechanics of Materials 42 (2010) 908-915. doi:10.1016/j.mechmat.2010.07.009

[79]. L H Xiao, X P Su, J H Wang, Y C Zhou. A novel blister test to evaluate the interface strength between nickel coating and low carbon steel substrate, Materials Science and Engineering A 501 (2009) 235-241. doi:10.1016/j.msea.2008.09.077

[80]. H Na, P Chen, Sh Wong. Adhesion Energy of Electrospun PVDF, Procedia Materials Science 1 (2012) 13-18. doi:10.1016/j.mspro.2012.06.003

[81]. M S Islam, L Tong. Effects of initial blister radius and shaft diameter on energy release rate of metal-polymer composite coating, Int. J. Adhesion & Adhesives 62 (2015) 107-123. doi:10.1016/j.ijadhadh.2015.07.007

[82]. J Sun, Y Lian, Zh Li, X He, Zh Zheng. Theoretical study on shaft-loaded blister test technique: Synchronous characterization of surface and interfacial mechanical properties, Intern. J. Adhesion & Adhesives 51 (2014) 128-139. doi:10.1016/j.ijadhadh.2014.03.004

[83]. T Guo, J He, X Pang, A A Volinsky, Y Su, L Qiao. High temperature brittle film adhesion measured from annealing-induced circular blisters, Acta Materialia 138 (2017) 1-9. doi:10.1016/j.actamat.2017.07.026

[84]. R E Galindo, A Van Veen, J H Evans, H Schut, J Th M de Hosson. A modified blister test to study the adhesion of thin coatings based on local helium ion implantation, Thin Solid films 471 (2005) 170-176. doi:10.1016/j.tsf.2004.06.129

[85]. D Wu, H Xie, H Wang, J Zhang and Ch Li. Dynamic buckling behaviour of thin metal film lines from substrate, J. Micromech. Microeng. 24 (2014) 105008 (6pp). doi:10.1088/0960-1317/24/10/105008

[86]. M Kappes, G S Frankel, N Sridhar. Adhesion and adhesion degradation of a pressure sensitive tape on carbon steel, Progress in Organic Coatings 69 (2010) 57-62. doi:10.1016/j.porgcoat.2010.05.005

[87]. B C Rincon Troconis, g S Frankel. Effect of roughness and surface topography on adhesion of PVB to AA2024-T3 using the blister test, Surface & coatings Technologyn236 (2013) 531-539. doi:10.1016/j.surfcoat.2013.10.046

[88]. Z Wang, Z Ma, Y Zhou, Ch Lu. Determination of interfacial adhesive properties for polymeric film by blister test, Trans. Nonferrous Mat. Soc. China 23 (2013) 3033-3039. doi: 10.1016/S1003-6326(13)62830-7

[89]. K Mahan, D Rosen, B Han. Blister testing for adhesion strength measurement of polymer films subjected to environmental conditions, J. Electronic Packaging 138 (2016) 041003 (9pp). doi: 10.1115/1.4034454

[90]. B W Hailesilassie, M N Partl. Adhesive blister propagation under an orthotropic bituminous waterproofing membrane, Construction and Building Materials 48 (2013) 1171-1178. doi:10.1016/j.conbuildmat.2013.07.047

[91]. D J Mills, S S Jamali. The best tests for anti-corrosive paints. And why: A personal viewpoint, Progress in Organic Coatings 102 (2017) 8-17. doi:10.1016/j.porgcoat.2016.04.045
[92]. E D Schachinger, R Braidt, B Strauβ, A W Hassel. EIS study of blister formation on coated galvanised steel in oxidising alkaline solutions, Corrosion Science 96 (2015) 5-13. doi: 10.1016/j.corsci.2014.12.010
[93]. R M Souto, Y González-García, S González, G âT Burstain. Imaging the origins of coating degradation and blistering caused by electrolyte immersion assisted by SECM, Electroanalysis 21 (2009) 2569-2574.DOI: 10.1002/elan.200900262
[94]. R M Souto, Y González-García, S González. Characterization of coating systems by scanning electrochemical microscopy: Surface topology and blistering, Progress in Organic Coatings 65 (2009) 435-439. doi:10.1016/j.porgcoat.2009.03.008
[95]. R M Souto, Y González-García, S González, G T Burstain. Damage to paint coatings caused by electrolyte immersion as observed in situ by scanning electrochemical microscopy, Corrosion Science 46 (2004) 2621-2628. doi:10.1016/j.corsci.2004.06.002
[96]. ISO 17093. Corrosion of metals and alloys, Guidelines for corrosion test by electrochemical noise measurements, 2015.
[97]. ISO 16773-1. Paints and varnishes electrochemical impedance spectroscopy (EIS) on high-impedance coated specimens. Part 1: Terms and definitions, 2016.
[98]. ISO 16773-2. Electrochemical impedance spectroscopy (EIS) on coated and uncoated metallic specimens, Part 2: Collection of data, 2016.
[99]. ISO 16773-3. Electrochemical impedance spectroscopy (EIS) on coated and uncoated metallic specimens, Part 3: Processing and analysis of data from dummy cells, 2016.
[100]. ISO 16773-4. Electrochemical impedance spectroscopy (EIS) on coated and uncoated metallic specimens. 2017.
[101]. ISO 17463. Paints and varnishes- Guidelines for the determination of anticorrosive properties of organic coatings by accelerated cyclic electrochemical technique, 2014.
[102]. Y He, G Y Tian, M Pan, D Chen, H Zhang. An investigation into eddy current pulsed thermography for detection of corrosion blister, Corrosion Science 78 (2014) 1-6. doi:10.1016/j.corsci.2013.09.001
[103]. B Eren, L Marot, G Günzburger, P-O Renault, Th Glatzel, R Steiner and E Meyer.Hydrogen-induced buckling of gold film, J. Phys. D: Appl. Phys. 47 (2014) 025302. doi:10.1088/0022-3727/47/2/025302
[104]. R A J M van den Bos, C J Lee, J P H Benschop and F Bijkerk. Blister formation in Mo/Si multi-layered structures induced by hydrogen ions, J. Phys. D: Appl. Phys. 50 (2017) 265302. doi:10.1088/1361-6463/aa7323
[105]. A S Kuznetsov, M A Gleeson and F Bijkerk. Hydrogen-induced blistering mechanisms in thin film coatings, J. Phys.: Condens. Matter 24 (2012) 052203. doi:10.1088/0953-8984/24/5/052203
[106]. W Zhu, Y C Zhou, J W Guo, L Yang, C Lu. Quantitative characterization of the interfacial adhesion of Ni thin film on steel substrate: a compression-induced buckling delamination test, Journal of the Mechanics and Physics of Solids 74 (2015) 19-37. doi:10.1016/j.jmps.2014.09.012
[107]. Ch Wang, J Kang, Zh Xue, H Tan. Buckling induced delamination and microflow analysis of film/substrate system, Composite Structures 161 (2017) 8-14.doi: 10.1016/j.compstruct.2016.11.045
[108]. Z Cao, P Wang, W gao, L Tao, J W Suk, R S Ruoff, D Akinwande, R Huang, K M Liechti. A blister test for interfacial adhesion of large-scale transferred graphene, Carbon 69 (2014) 390-400. doi:10.1016/j.carbon.2013.12.041
[109]. H Xin, R Borduin, W Jiang, K M Liechti, W Li. Adhesion energy of as-grown graphene on copper foil with a blister test, Carbon 123 (2017) 243-249. doi:10.1016/j.carbon.2017.07.053
[110]. J S Bunch, M L Dunn. Adhesion mechanics of graphene membranes. Solid State Communications 152 (2012) 1359-1364. doi:10.1016/j.ssc.2012.04.029
[111]. Z Zong, Ch Chen, M R Dokmeci, K Wan. Direct measurement of graphene adhesion on silicon surface by intercalation of nanoparticles, J. Appl. Phys. 107 (2010) 026104. doi:10.1063/1.3294960

[112]. G Li, C Yilmaz, X An, Si Somu, S Kar, Y J Jung, A Busnaina, and K Wan. Adhesion of graphene sheet on nano-patterned substrates with nano-pillar array, J. Appl. Phys. 113 (2013) 244303. doi:10.1063/1.4811718

[113]. S P Koenig, N G Boddeti, M L Dunn and J S Bunch. ultrastrong adhesion of graphene membranes, Nat. Nanotechnol. 6 (2011) 543-546. doi: 10.1038/NNANO.2011.123

[114]. D Metten, F Federspiel, M Romeo,and S Berciaud. All-optical blister test of suspended graphene using micro-Raman spectroscopy, Phys. Rev. Appl. 2 (2014) 054008. doiI: 10.1103/PhysRevApplied.2.054008

[115]. A Fedorov and J Th M De Hosson. Adhesion of polymer coating studied by laser-induced delamination, J. Appl. Phys. 97 (2005) 123510. doi:10.1063/1.1929858

[116]. A Kleinbichler, J Zechner, M J Codill. Buckle induced delamination techniques to measure the adhesion of metal dielectric interfaces, Microelectronic Engineering 167 (2017) 63-68. doi:10.1016/j.mee.2016.10.020

[117]. Y Liang, X Bi and J Wang. Numerical simulation of laser-induced thin film delamination, Thin Solid Films 516 (2008) 971-981. doi:10.1016/j.tsf.2007.06.066

[118]. L Berthe, M Arrigoni, M. Boustie , J. P. Cuq-Lelandais , C. Broussillou , GFabre , M. Jeandin , V. Guipont & M. Nivard. State-of-the-laser adhesion test (LASAT), Nondestructive Testing & Evaluation, 25 (2011) 303-317. doi: 10.1080/10589759.2011.573550

[119]. S S V Kandula. Laser based adhesion testing technique to measure thin film-substrate interface toughness in Laser Technology: applications in Adhesion and Related areas (2017) 269-298 doi:10.1002/9781119185031

[120]. V Gupta and A S Argon. Measurement of interface strength by laser-pulse-induced spallation, Materials Science & Engineering A126 (1990) 105-117. doi: 10.1016/0921-5093(90)90116-K

[121]. J Shim, E Hagerman, B Wu and V Gupta. Measurement of the tensile strength of cell-biomaterial interface using the laser spallation technique, Acta Biomaterialia 4 (2008) 1657-1668. doi:10.1016/j.actbio.2008.06.001

[122]. S Barradas, R Molins, M Jeandin, M Arrigoni, M Boustie, C Bolis, L Berthe, M Ducos. Application of laser shock adhesion testing to the study of the interlamellar strength and coating-substrate adhesion in cold-sprayed copper coating of aluminium, Surface & Coating Technology 197 (2005) 18-27. doi:10.1016/j.surfcoat.2004.08.222

[123]. J Radziejewska, A Sarzynski, M Strzelec, R. Diduszko, J. Hoffman. Evaluation of residual stress and adhesion of Ti and TiN PVD films by laser spallation technique, Optics and Laser Technology, 104(2018) 140-147. doi: 10.1016/j.optlastec.2018.02.014

[124]. O T Kingstedt and J Lambros, Ultra-high speed imaging of laser-induced spallation. *Expl. Mech.* 55 (2015) 587–598. doi:10.1007/s11340-014-9973-0

[125]. R Ikeda, H Cho, A Sawabe, M Takemoto. Laser spallation method to measure strength against Mode-I decohesion of CVD diamond film, Diamond & Related Materials 14 (2005) 631-636. doi:10.1016/j.diamond.2004.11.025

[126]. D Schneider. Using laser induced surface acoustic waves to characterize thin films and material surfaces, IEEE International Ultrasonics Symposium Proceedings (2012) 270-272. doi: 10.1109/ULTSYM.2012.0066

[127]. Y Watanabe, Sh Fujisawa, A Yonezu, X Chen. Quantitative evaluation of adhesion quality of surface coating by using pulse laser-induced ultrasonic waves, Surface & Coatings Technology 286 (2016) 231-238. doi:10.1016/j.surfcoat.2015.12.026

[128]. L Hu, P Miller, J Wang**,** High strain-rate spallation and fracture of tungsten by laser-induced stress wave. Materials Science and Engineering A 504 (2009) 73-80. doi:10.1016/j.msea.2008.10.048

[129]. M Arai, Y Sato, D Sugiura, M Nishimura, H Ito. Inverse analysis for interface fracture toughness of Ti coating film by laser spallation method, Advanced in Engineering software 000 (2016) 1-6. doi: 10.1016/j.advengsoft.2016.04.003

[130]. M Perton, A Blouin, J-P Monchalin. Adhesive bond testing of carbon-epoxy composites by laser shockwave, J. Phys. D: Appl. Phys. 44 (2011) 034012. doi:10.1088/0022-3727/44/3/034012

[131]. R Ecault, M Boustie, F Touchard, F Pons, L Berthe, L Chocinski-Arnault, B Ehrhart, C Bockenheimer. A study of composite material damage induced by laser shock wave, Composites: Part A 53 (2013) 54-64. doi:10.1016/j.compositesa.2013.05.015

[132]. B Ehrhart, R Ecault, F Touchard, M Boustie, L Berthe, C Bockenheimer, B Valeske. Development of a laser shock adhesion test for the assessment of weak adhesive bonded CFRP structures, Intern. J. Adhesion & Adhesives 52 (2014) 57-65. doi: 10.1016/j.ijadhadh.2014.04.002

[133]. E Gay, L Berthe, M Boustie, M Arrigoni, M Trombini. Study of the response of CFRP composite laminates to a laser-induced shock, Composites: Part B 64 (2014) 108-115. doi:10.1016/j.compositesb.2014.04.004

[134]. R Ecault, F Touchard, M Boustie, L Berthe, N Dominguez. Numerical modelling of laser-induced shock experiments for the development of the adhesion test for bonded composite materials, Composite Structures 152 (2016) 382-394. doi:10.1016/j.compstruct.2016.05.032

[135]. A R Rafieerad, A R Bushroa, B Nasiri-Tabrizi, R Crum, C G_amez, J Vadivelu, V. Gupta. Vertically oriented ZrO_2-Tio_2-Nb_2O_5-Al_2O_3 mixed nanopatterned bioceramics on Ti6Al7Nb implant assessed by laser spallation technique, J. Alloys & Compounds 721 (2017) 456-475. doi:10.1016/j.jallcom.2017.05.225

[136]. D Courapied, L Berthe, P Peyre, F Coste J-P Zou and A-M Sautivet. Laser-delayed double shock-wave generation in water-confinementregime, Journal of Laser Application 27 (2015) S29101. doi:10.2351/1.4906382

[137]. D Courapied, R Kromer, L Berthe, P Peyre, S Costil, J Cormier, M Boustie, and X Milhet. Laser adhesion test for thermal sprayed coatings on textured surface by laser. Journal of Laser Applications 28 (2016) 022509. doi: 10.2351/1.4944451

[138]. J Wang, N R Sottos, R L Weaver. Tensile and mixed-mode strength of a thin film-substrate interface under laser induced pulse loading, Journal of the Mechanics and Physics of Solids 52 (2004) 999-1022. doi:10.1016/j.jmps.2003.09.029

[139]. R Kitery, Ph H Geubelle, N R Sottos. Mixed-mode interfacial adhesive strength of a thin film on an anisotropic substrate, Journal of the Mechanics and Physics of Solids 57 (2009)51-66. doi:10.1016/j.jmps.2008.10.002

[140]. Ph Tran, S S Kandula, P H Geubelleand N R Sottos. Comparison of dynamic and quasi-static measurements of thin film adhesion, J. Phys. D: Appl. Phys. 44 (2011) 034006.doi:10.1088/0022-3727/44/3/034006

[141]. G Bégué, G Fabre, V Guipont, M Jeandin, P Bilhe, JY Guédou, F Lepoutre. Laser shock adhesion test (LASAT) of EB-PVD TBCs: towards and industrial application, Surface & Coatings Technology 237 (2013) 305-312. doi:10.1016/j.surfcoat.2013.07.026

[142]. H Sapardanis, V Maurel, A Köster, S Duvinage, F Borit, V Guipont. Influence of macroscopic shear loading on the growth of an interfacial crack initiated from a ceramic blister processed by laser shock, Surface & coatings Technology 291 (2016) 430-443. doi:10.1016/j.surfcoat.2016.02.050

[143]. X Cheng, H Jiao, J Lu, B Ma, and Zh Wang. Nanosecond pulsed laser damage characteristics of HfO2/SiO2 high reflection coatings irradiated from crystal-film interface, Optics Express 21 (2013) 14867. doi:10.1364/OE.21.014867

[144]. J Di, M Zhou, J Li, Ch Li, W Zhang, G Amoako. Micro-punching process based on spallation delamination induced by laser driven-flyer, Applied Surface Science 258 (2012) 2339-2343. doi:10.1016/j.apsusc.2011.10.018

[145]. N W Khun, B C Rincon Troconis, G S Frankel. Effects of carbon nanotube content on adhesion strength and wear and corrosion resistance of epoxy composite coatings on AA2014-T3, Progress in Organic Coatings 77 (2014) 72-80. doi:10.1016/j.porgcoat.2013.08.003

[146]. M Arrigoni, S Barradas, M Braccini, M Dupeux, M Jeandin, M Boustie, C Bolis and L Berthe. A comparative study of three adhesion tests (EN 582, similar to ASTM C633, LASAT (LASer Adhesion Test), and bulge and blister test) performed on plasma sprayed copper deposited on aluminium 2017 substrates, Journal of Adhesion Science & Technology 20 (2006) 471-487. doi:10.1163/156856106777144336

[147]. The Japanese Society for Non-Destructive Inspection - Practical acoustic emission testing, Springer Japan 2016. doi:10.1007/978-4-431-55072-3

[148]. N Gierse, B Schweer, A Huber, O Karger, V Philipps, U Samm, G Sergienko. In situ characterisation of hydrocarbon layers in TEXTOR by laser induced ablation and laser induced breakdown spectroscopy. Journal of nuclear Materials 415 (2011) S1195-S1198. doi:10.1016/j.jnucmat.2010.11.055

[149]. X Xiao, H Qi, X Sui, T Kikkawa. Evaluation and criterion determination of the low-k thin film adhesion by the surface acoustic waves with cohesive zone model, Appl. Surf. Sci. 399 (2017) 599-607. doi: 10.1016/j.apsusc.2016.12.005

[150]. M Nikbakht, J Yousefi, H osseini-Toudeshky, G Minak. Delamination evaluation of compositelaminates with different interface fibre orientations using acoustic emission features and micro visualization, Composites Part B 113 (2017) 185-196. doi:10.1016/j.compositesb.2016.11.047

[151]. L. Yang, Y.C. Zhou, C. Lu. Damage evolution and rupture time prediction in thermal barrier coatings subjected to cyclic heating and cooling: An acoustic emission method, Acta Materialia 59 (2011) 6519–6529. doi:10.1016/j.actamat.2011.06.018

[152]. W. B. Yao, C.Y. Dai, W G Mao, C Lu, L Yang, Y C Zhou. Acoustic emission analysis on tensile failure of air plasma-sprayed thermal barrier coatings, Surface & Coatings Technology 206 (2012) 3803–3807. doi:10.1016/j.surfcoat.2012.03.050

[153]. E Mayrhofer, L Janka, W P Mayr, J Norpoth, M R Ripoll, M Gröschl. Cracking resistance of Cr_3C_2-NiCr and WC-Cr_3C_2-Ni thermally sprayed coatings under tensile bending stress. Surface & coatings Technology 281 (2015) 169-175. doi:10.1016/j.surfcoat.2015.09.002

[154]. G Li, Zh Zhang, H Wang, B Xu, Zh Piao, L Zhu. Acoustic emission monitoring and failure mechanism analysis of rolling contact fatigue for Fe-based alloy coating, Tribology International 61 (2013) 129–137. doi:10.1016/j.triboint.2012.12.010

[155]. Zh Piao, B Xu, H Wang, D Wen. Investigation of acoustic emission source of Fe-based sprayed coating under rolling contact, International Journal of Fatigue 47 (2013) 184–188. doi:10.1016/j.ijfatigue.2012.08.011

[156]. L Yang, T T Yang, Y C Zhou, Y G Wei, R T Wu, N G Wangl. Acoustic emission monitoring and damage mode discrimination of APS thermal barrier coatings under high temperature CMAS corrosion, Surface & Coatings Technology 304 (2016) 272-282. doi: 10.1016/j.surfcoat.2016.06.080

[157]. L. Yang, Z.C. Zhong, J You, Q M Zhang, Y C Zhou, W Z Tang. Acoustic emission evaluation of fracture characteristics in thermal barrier coatings under bending, Surface & Coatings Technology 232 (2013) 710–718. doi:10.1016/j.surfcoat.2013.06.085

[158]. M Zhou, W B Yao, X S Yang, Z B Peng, K K Li, C Y Dai, W G Mao, Y C Zhou, C Lu. In-situ and real-time tests on the damage evaluation and fracture of thermal barrier coatings under tension: A coupled acoustic emission and digital image correlation method, Surface & Coatings Technology 240 (2014) 50-47. doi: 10.1016/j.surfcoat.2013.12.010

[159]. S Nishinoiri, M Enoki, K tomita. Evaluation of Microfracture Mode in Ceramic coating during thermal cycle test using laser AE technique, Matierals Transactions 45 (2004) 92-101. doi:10.2320/matertrans.45.92

[160]. M Watanabe, M Enoki, T Kishi. Fracture behaviour of ceramic coatings during thermal cycling evaluated by acoustic emission method using laser interferometers, Materials Science & Engineering A 359 (2003) 368-374. doi:10.1016/S0921-5093(03)00394-0

[161]. P F Lowers, S Yoshida, K Gomi, S Adhikari, K Dreux, M Basnet, Ch Miyasaka, B R. Tittmann. Evaluation of thin film coating adhesion with an opto-acoustic technique, IEEE International Ultrasonics Symposium Proceedings (2011) 1103-1106.DOI: 10.1109/ULTSYM.2011.0271

[162]. S Yoshida, S Adhikari, K Gomi, R Shrestha, D Huggett, C Miyasaka, and I Park. Opto-acoustic technique to evaluate adhesion strength of thin-film systems, AIP Advances 2 (2012) 022126. doi:10.1063/1.4719698

[163]. R L Reuben. 13–Acoustic emission and ultrasound for monitoring the bone-implant interface, Bone Response to Dental Implant Materials (2017) 247-259. doi:10.1016/B978-0-08-100287-2.00013-6

[164]. E Agletdinov, E Pomponi, D Merson, A Vinogradov. A novel Bayesian approach to acoustic emission data analysis, Ultrasonics 72 (2016) 89–94. doi: 10.1016/j.ultras.2016.07.014

[165]. Luigi Calabrese, LucioBonaccorsi, M Galeano, E Proverbio, D D Pietro, F Cappuccini. Identification of damage evolution during SCC on 17-4 PH stainless steel by combining electrochemical noise and acoustic emission techniques, Corrosion Science 98 (2015) 573–584. doi:10.1016/j.corsci.2015.05.063

[166]. M R Neyra AStudillo,NicolásNúñez, M ILópez Pumarega, J Ruzzante, LPadovese. Magnetic Barkhausen noise and magneto acoustic emissionin stainless steel plates, Procedia Materials Science 8 (2015) 674 – 682. doi: 10.1016/j.mspro.2015.04.124

[167]. W D Callister Jr and D G Rethwisch. Materials Science and Engineering an Introduction, 9th Edition, Wiley, New Jersey, 2014.

[168]. T Guo, L Qiao, X Pang, A A Volinsky. Brittle film-induced cracking of ductile substrates, Acta Materialia 99 (2015) 273-280. doi: 10.1016/j.actamat.2015.07.059

[169]. Ch Zhang, L Gu, Ch Nie, Ch Zhang and L Wang. Interfacial mechanics analysis of a brittle coating – ductile substrate system involved in thermoelastic contact, coating 7 (2017) 21. doi:10.3390/coatings7020021

Figure(s)

Click here to download high resolution image

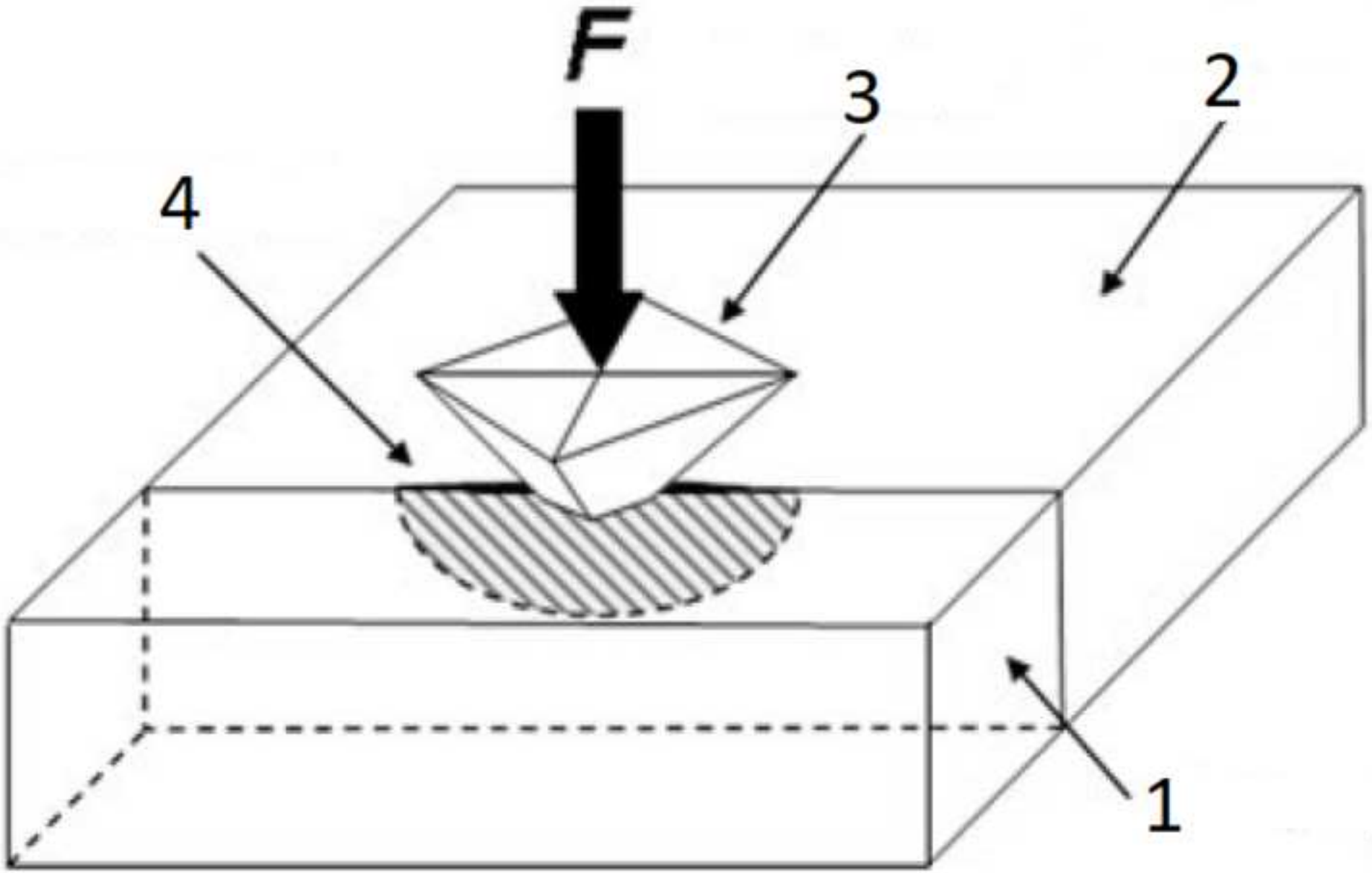

Figure(s)

Click here to download high resolution image

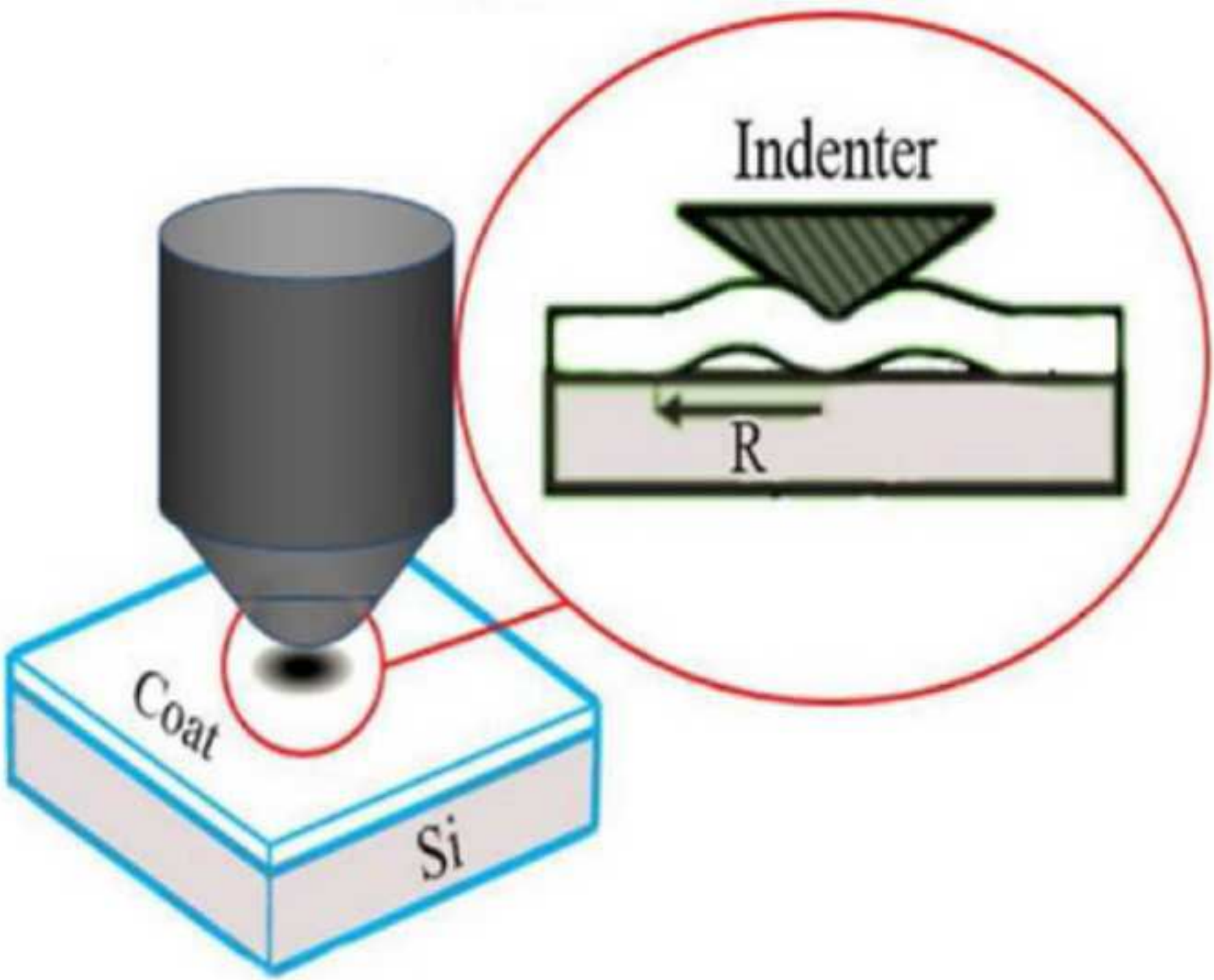

Figure(s)

Click here to download high resolution image

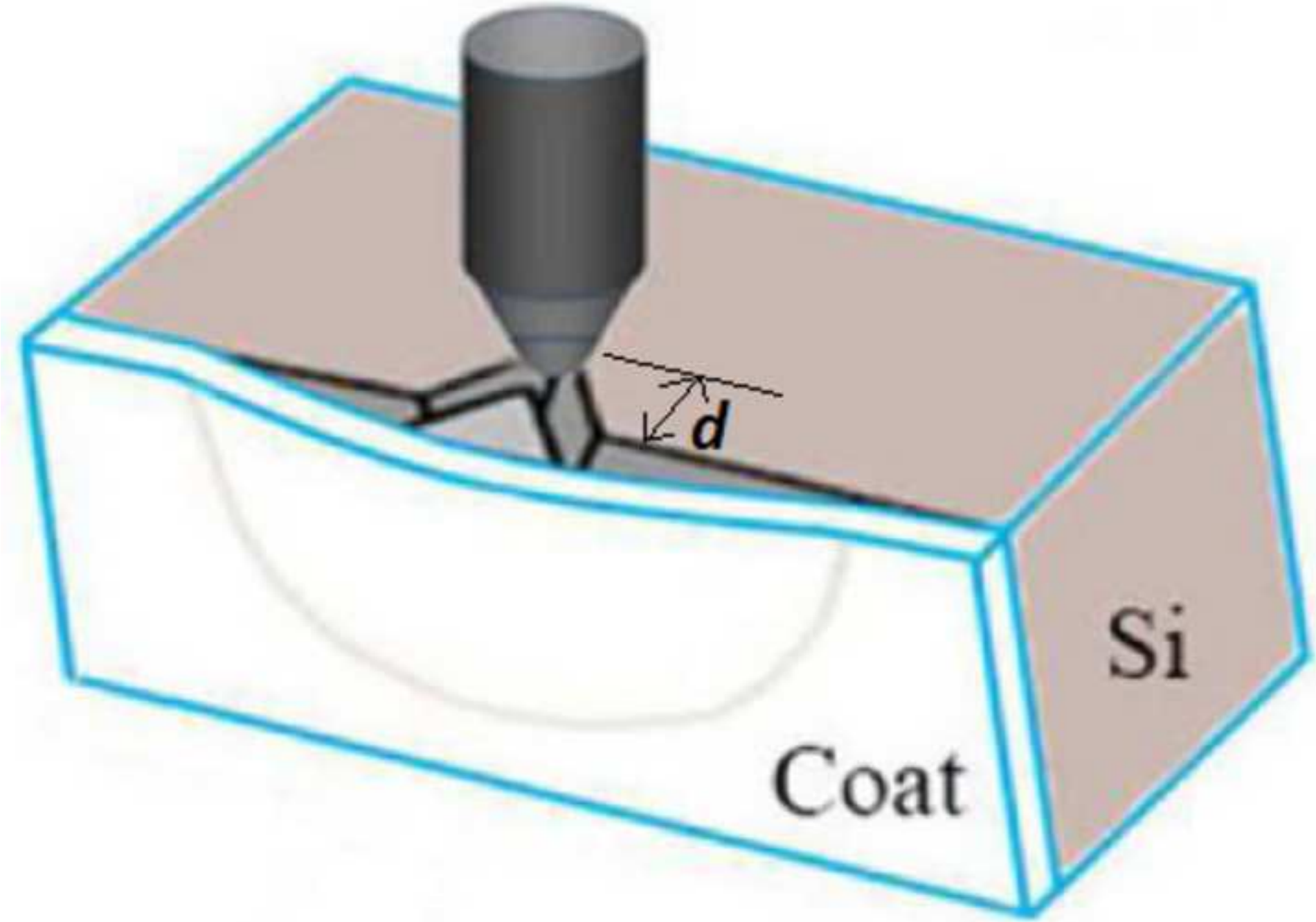

Figure(s)
Click here to download high resolution image

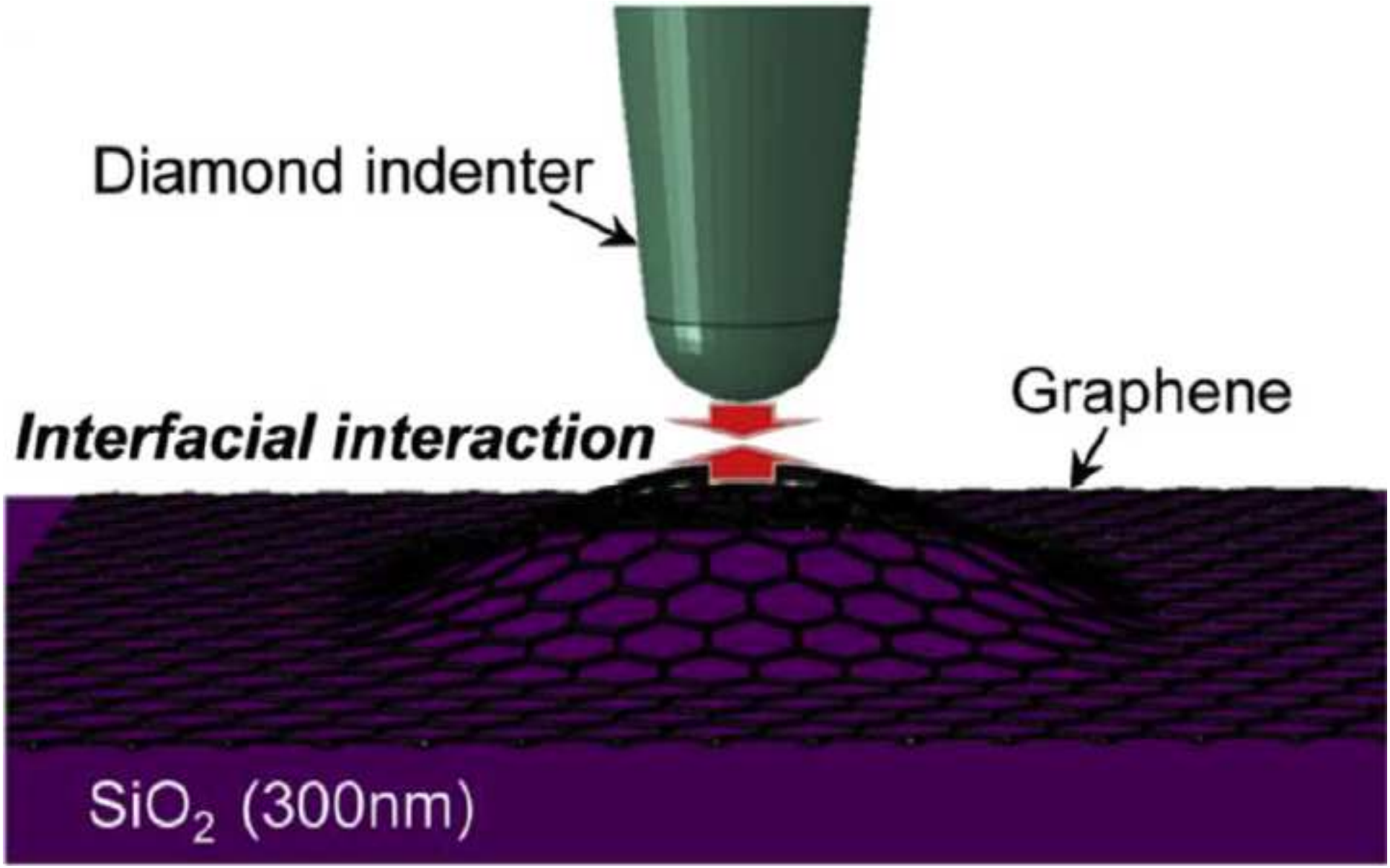

Figure(s)
Click here to download high resolution image

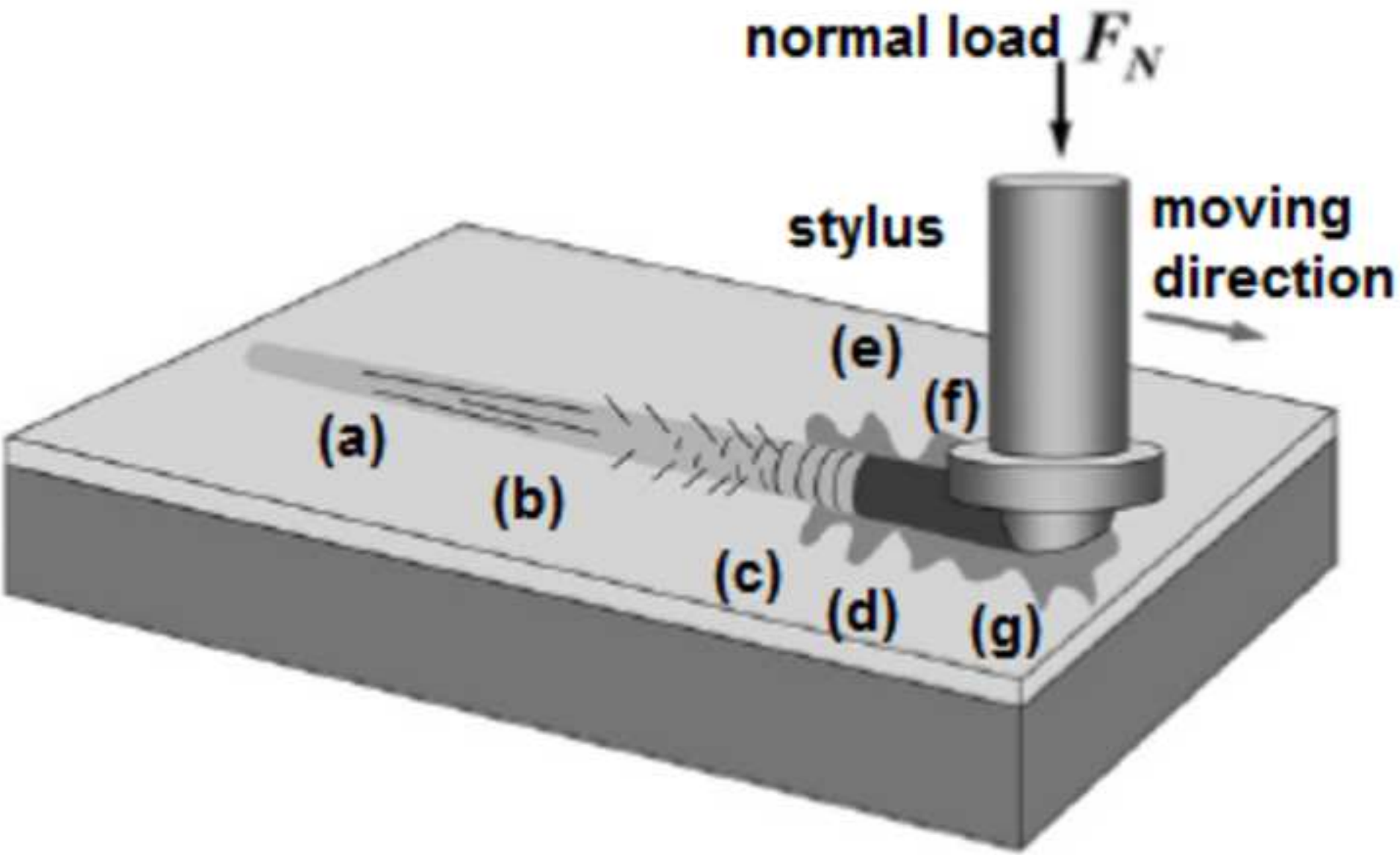

Figure(s)
Click here to download high resolution image

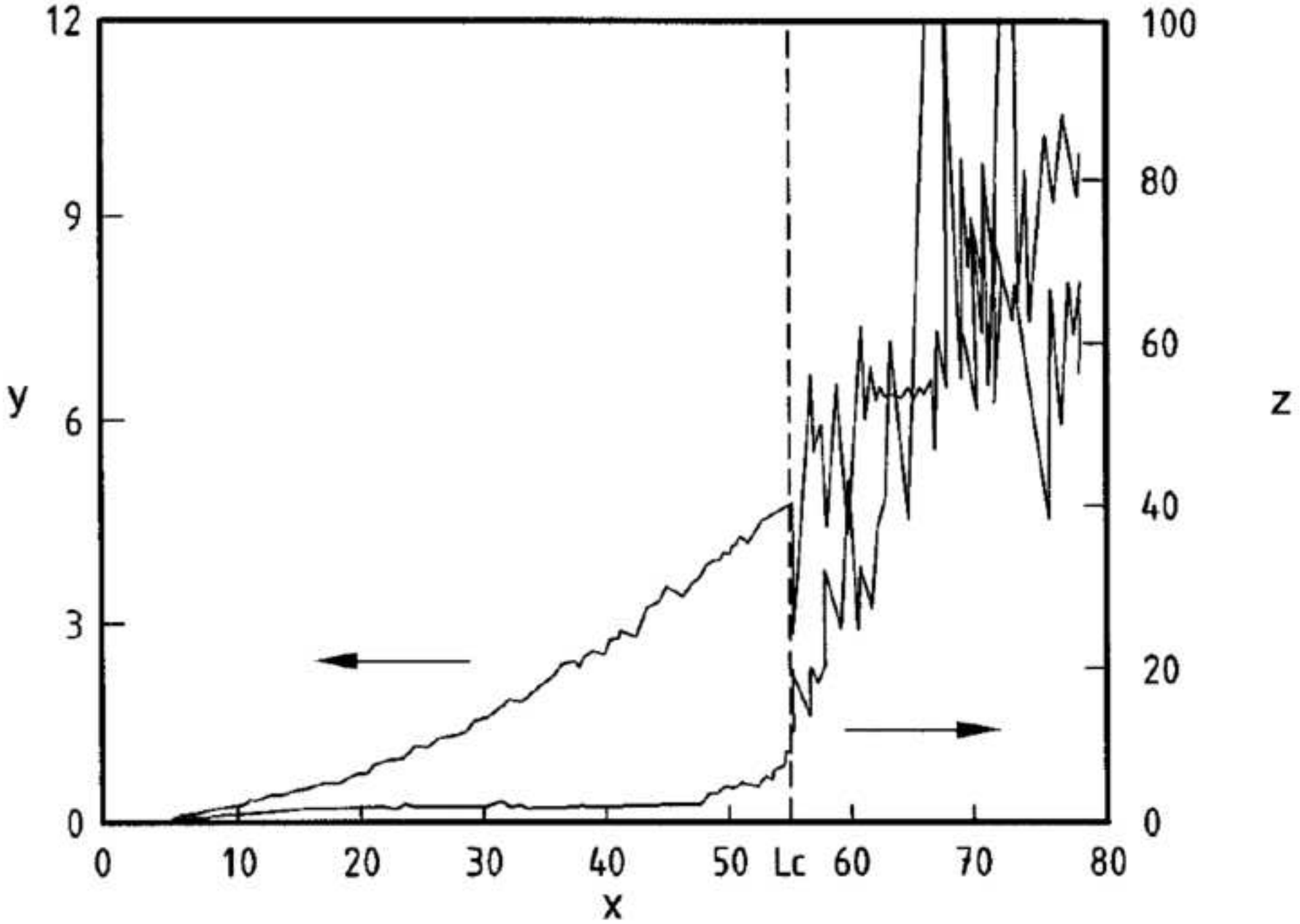

Figure(s)
Click here to download high resolution image

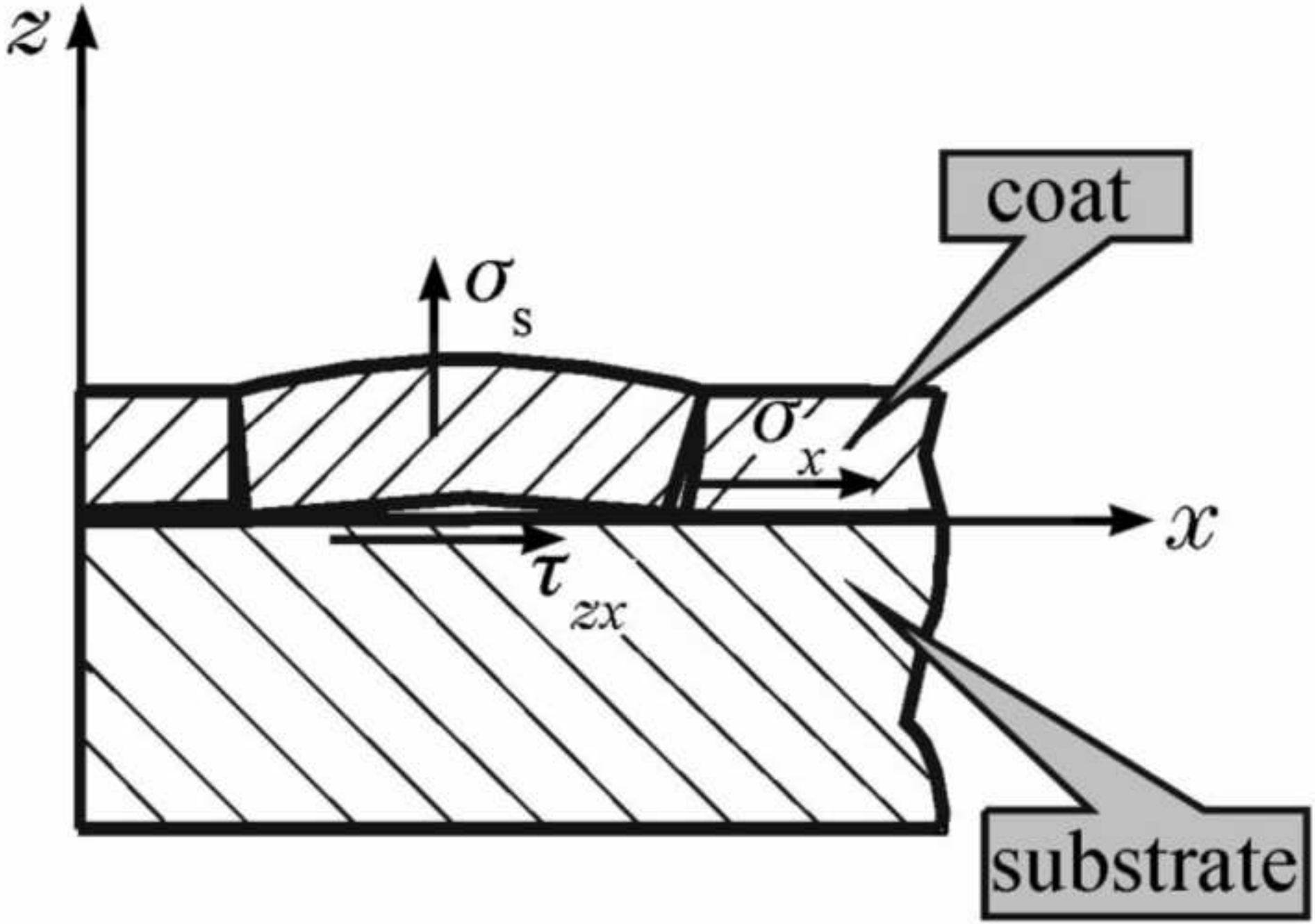

Figure(s)

Click here to download high resolution image

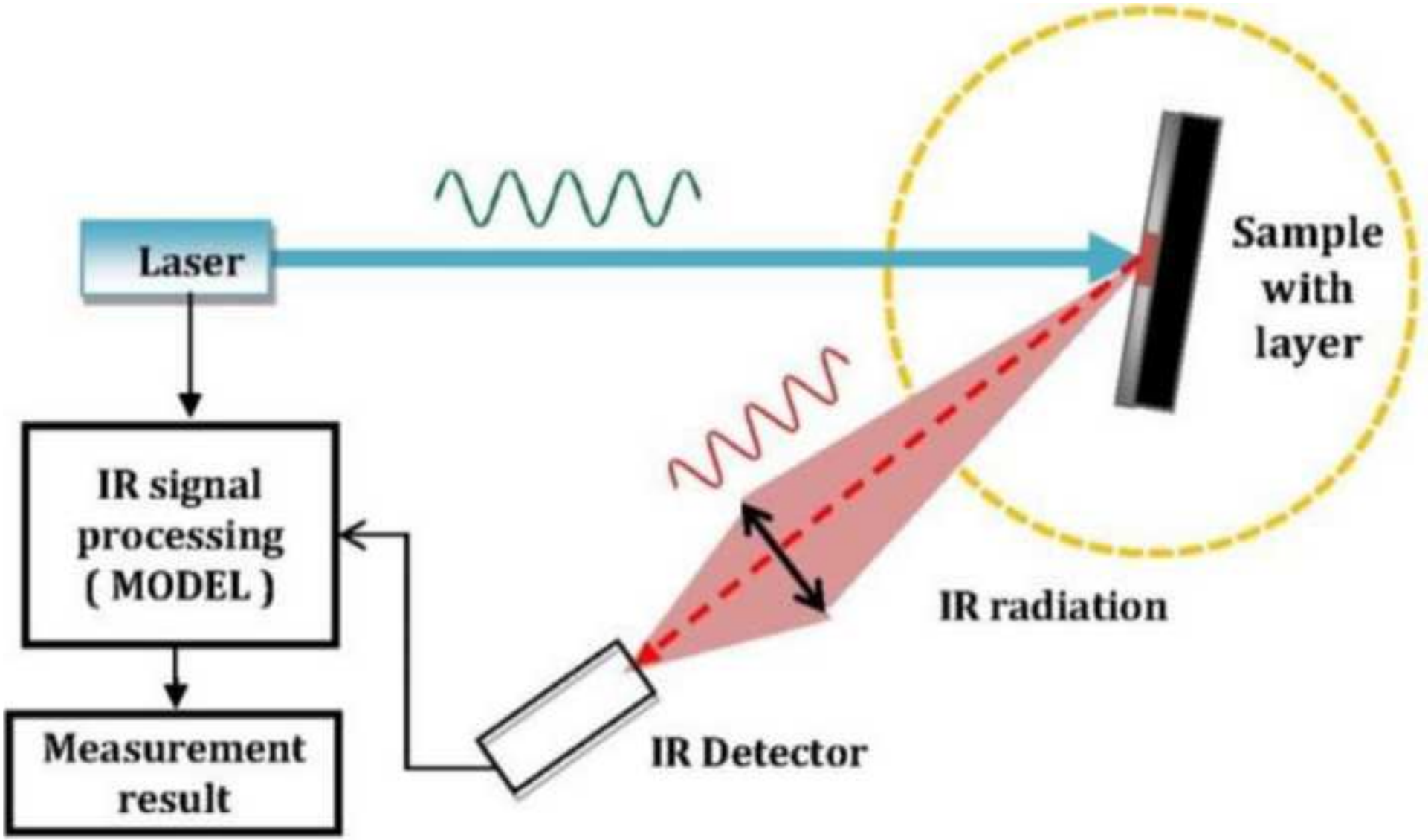

Figure(s)

Click here to download high resolution image

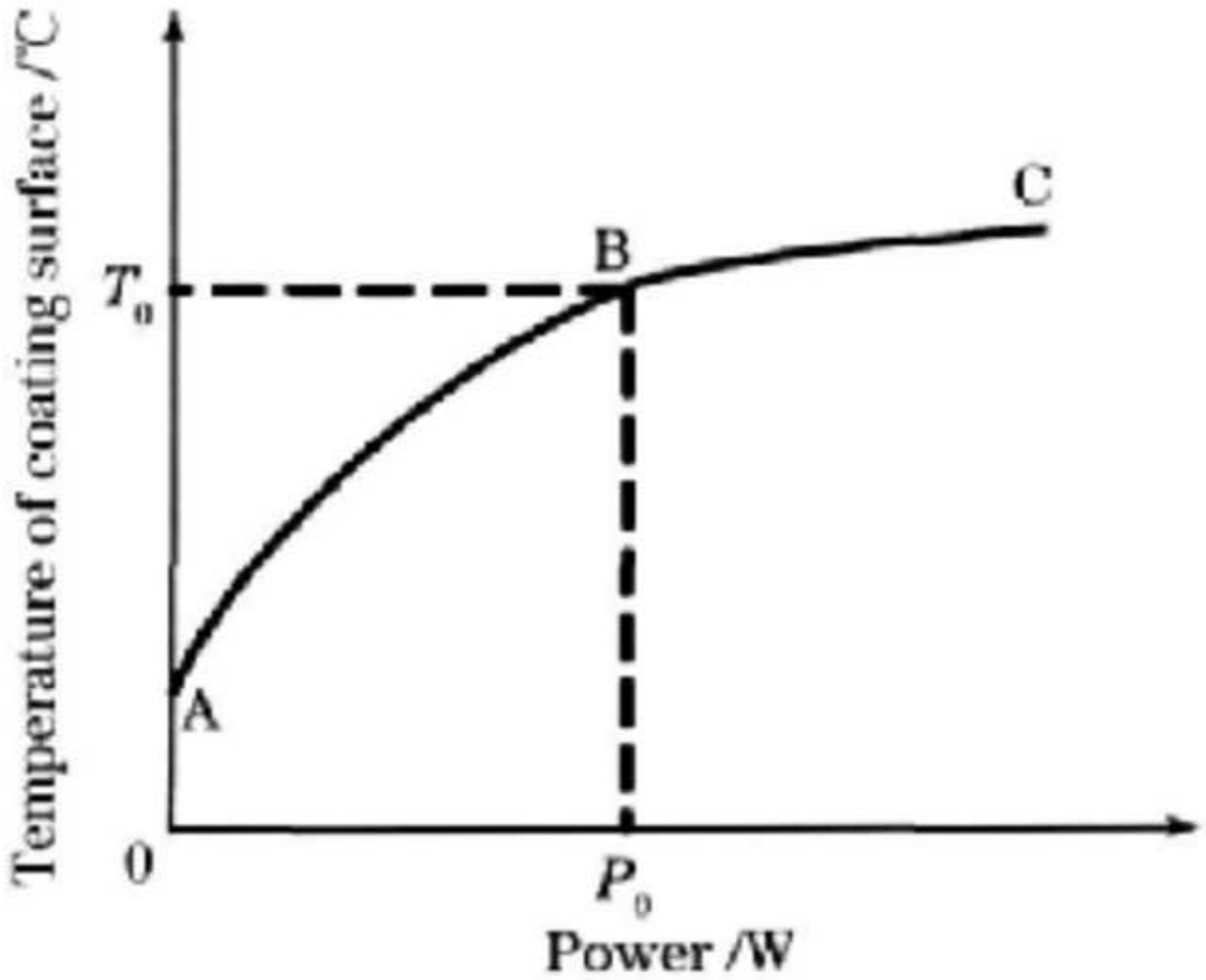

Figure(s)

Click here to download high resolution image

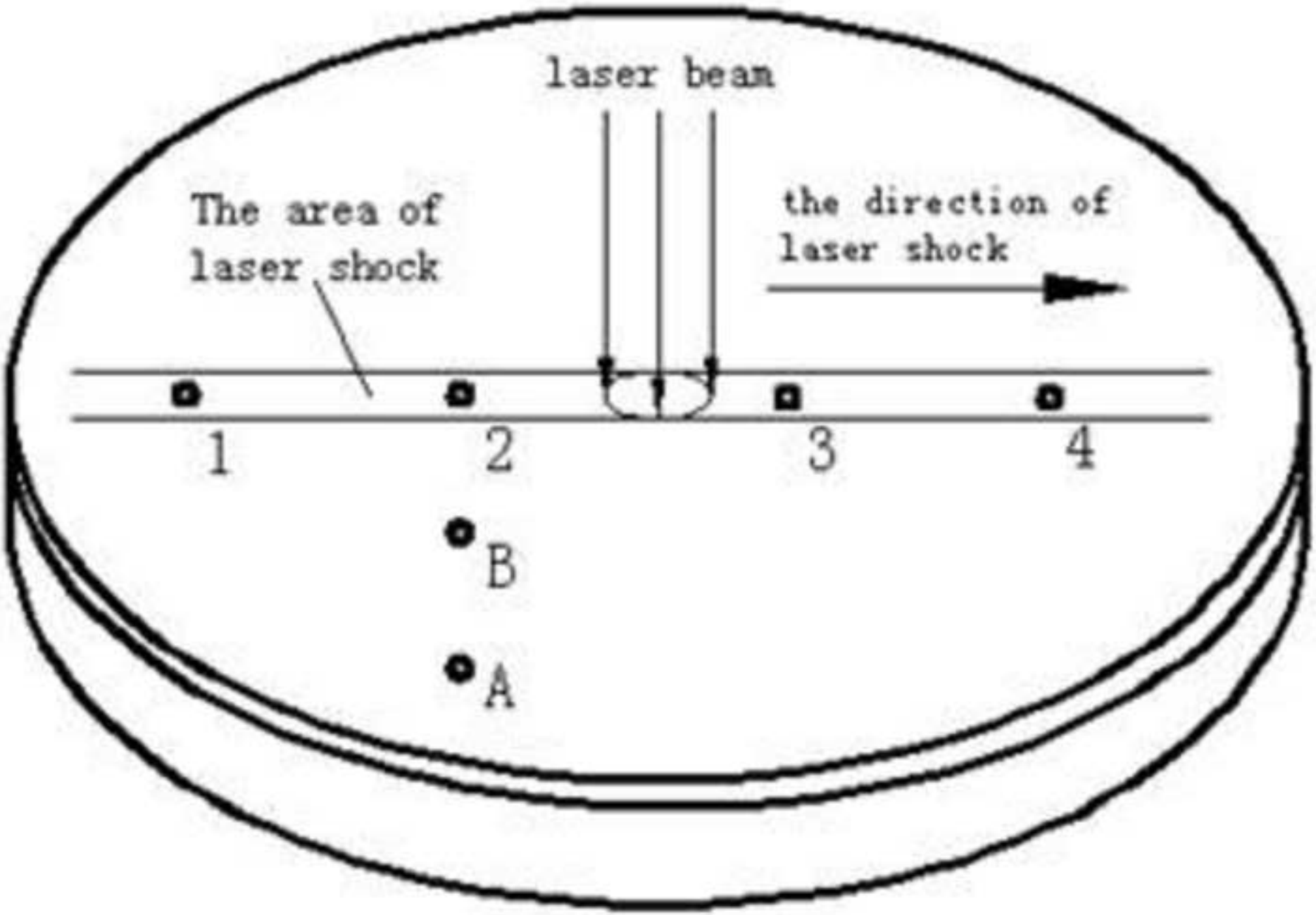

Figure(s)
Click here to download high resolution image

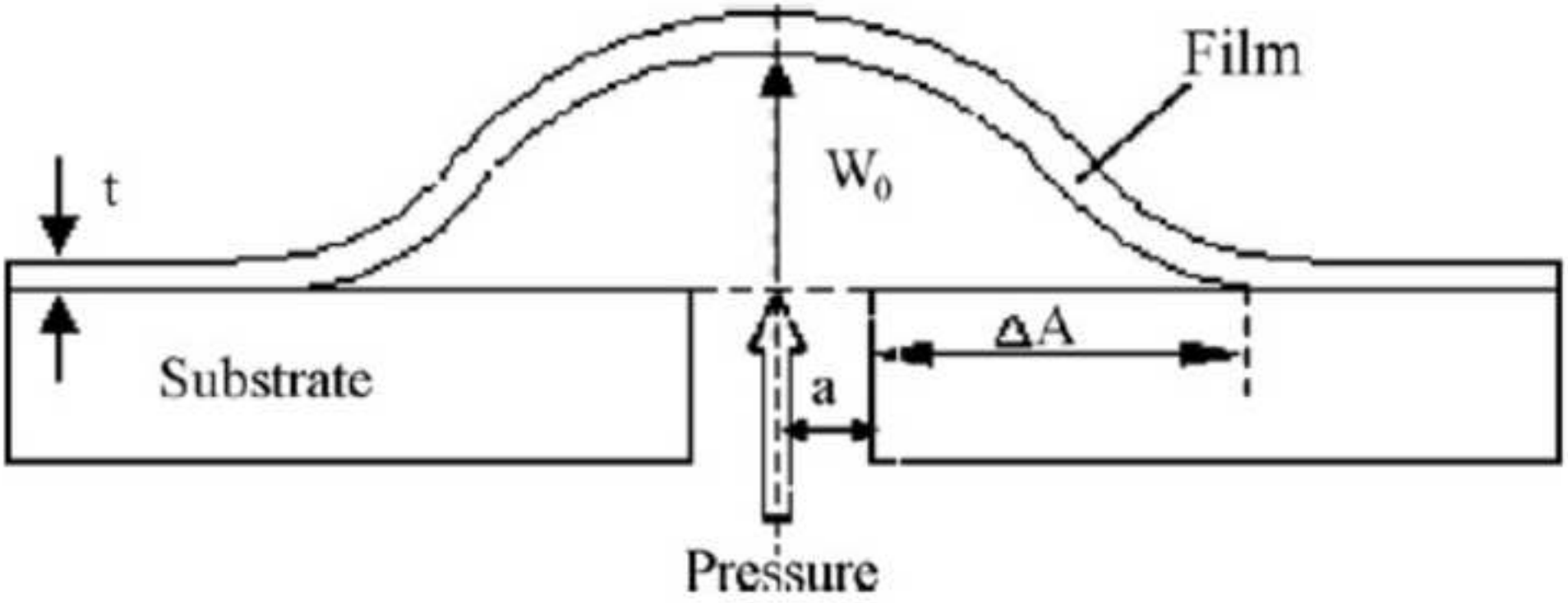

Figure(s)
Click here to download high resolution image

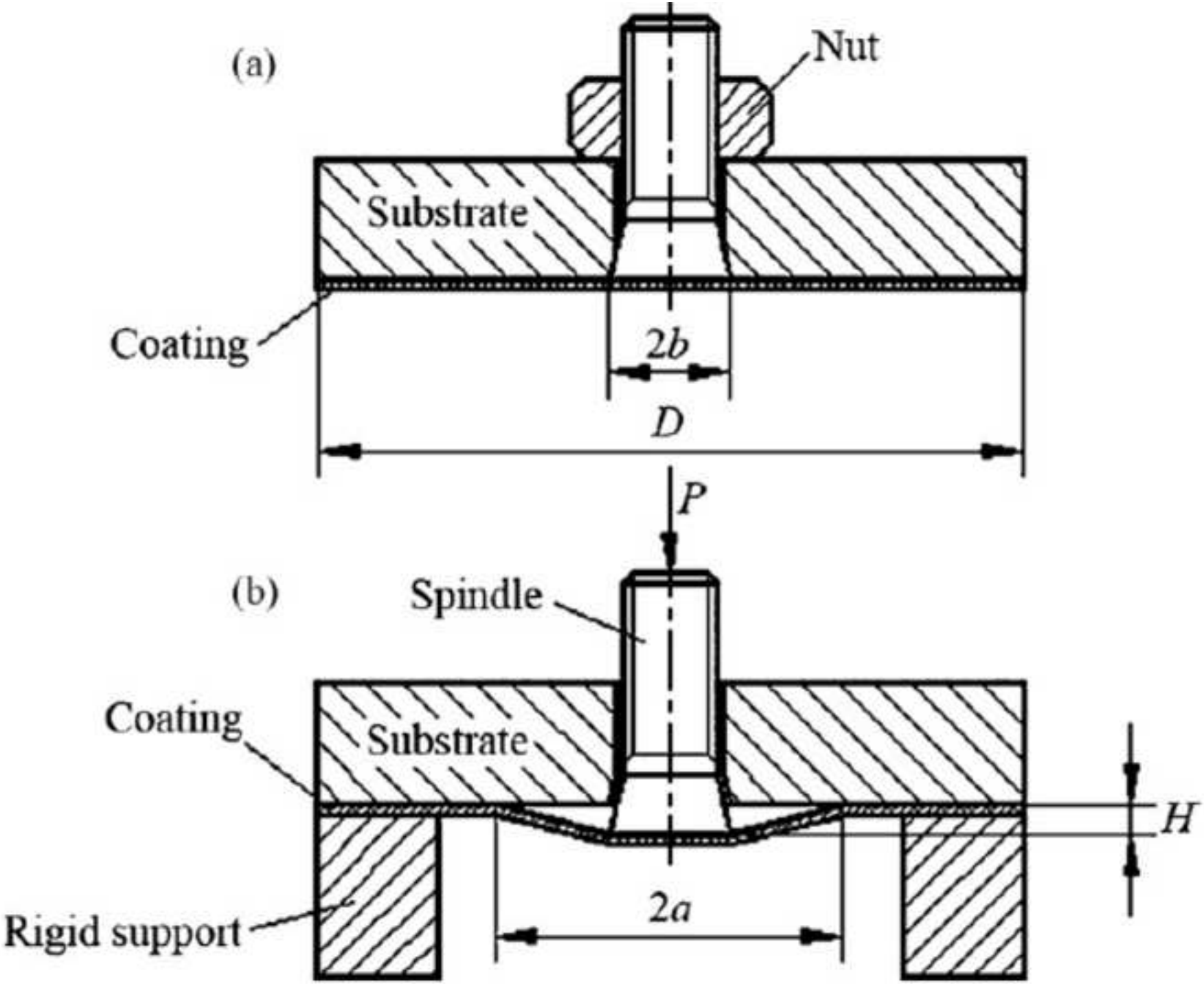

Figure(s)
Click here to download high resolution image

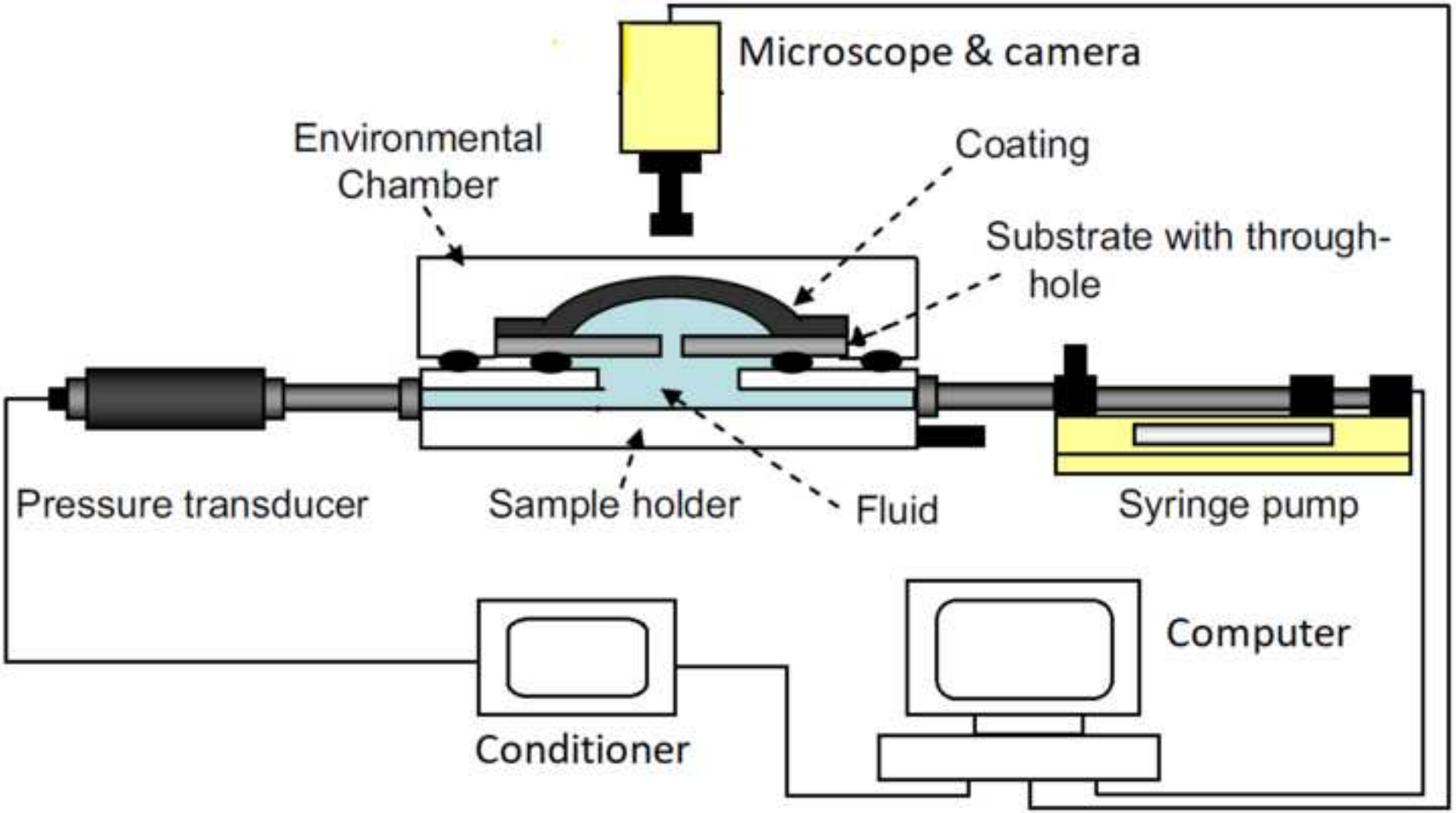

Figure(s)
Click here to download high resolution image

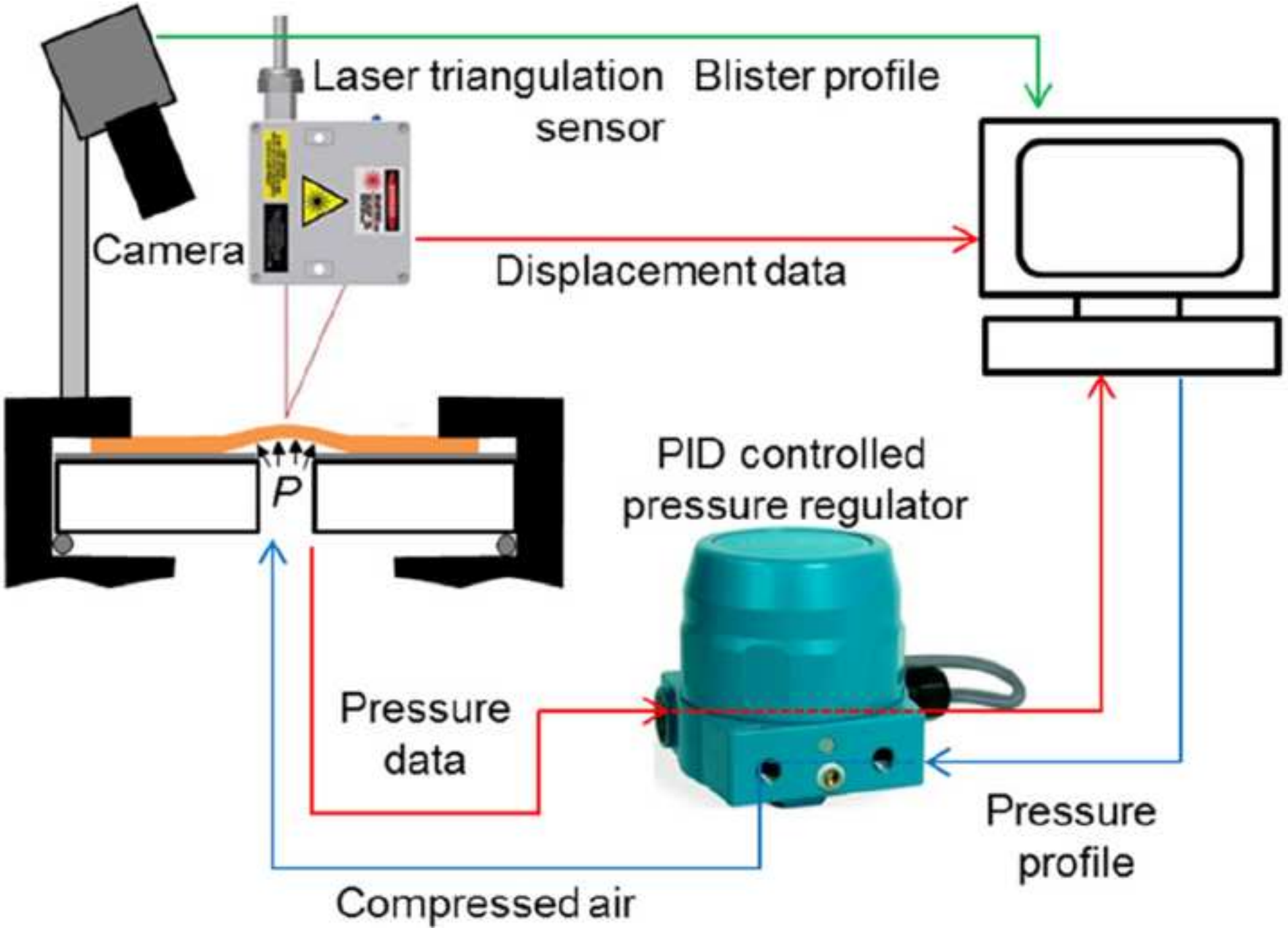

Figure(s)

Click here to download high resolution image

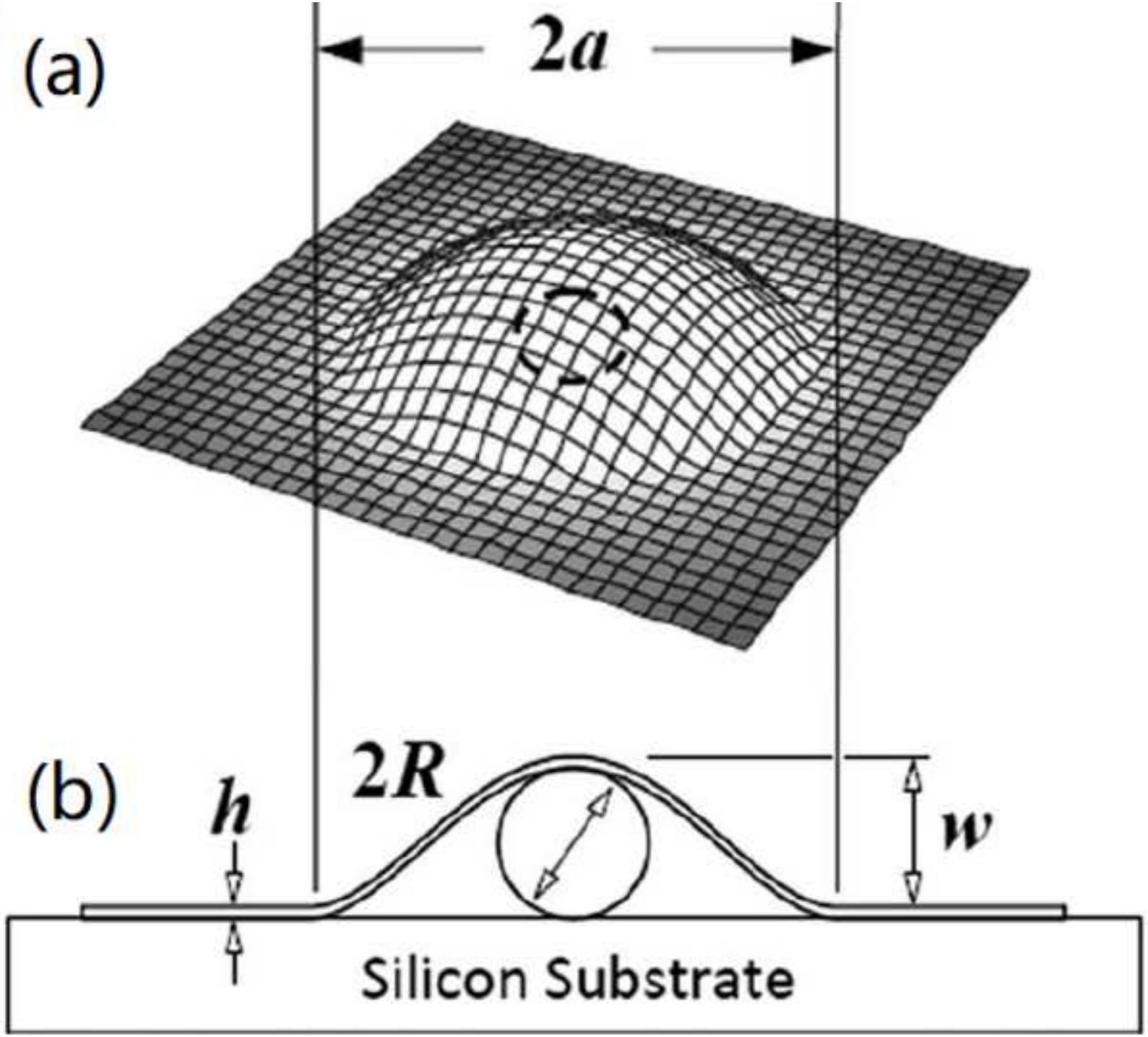

Figure(s)
Click here to download high resolution image

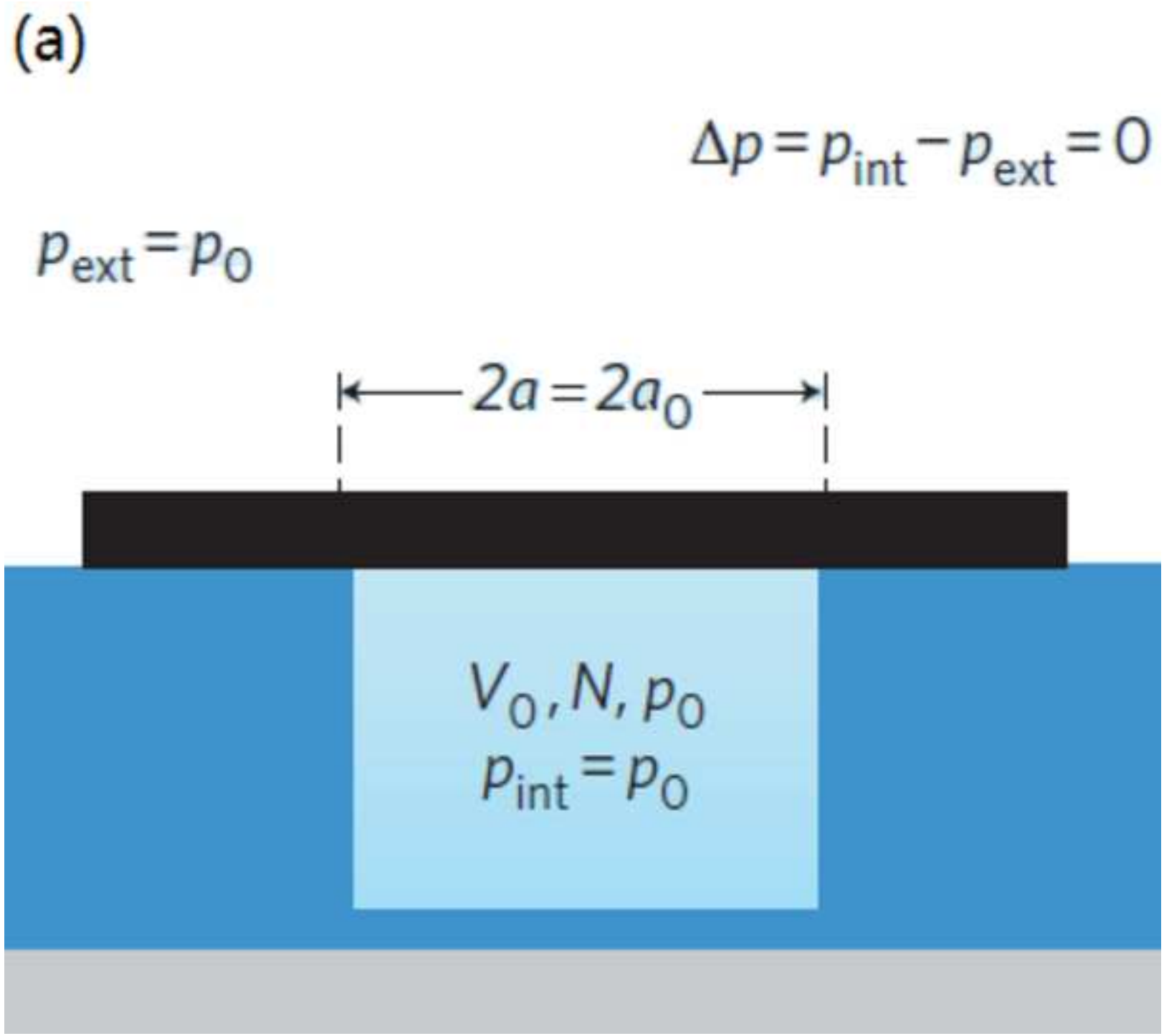

Figure(s)
Click here to download high resolution image

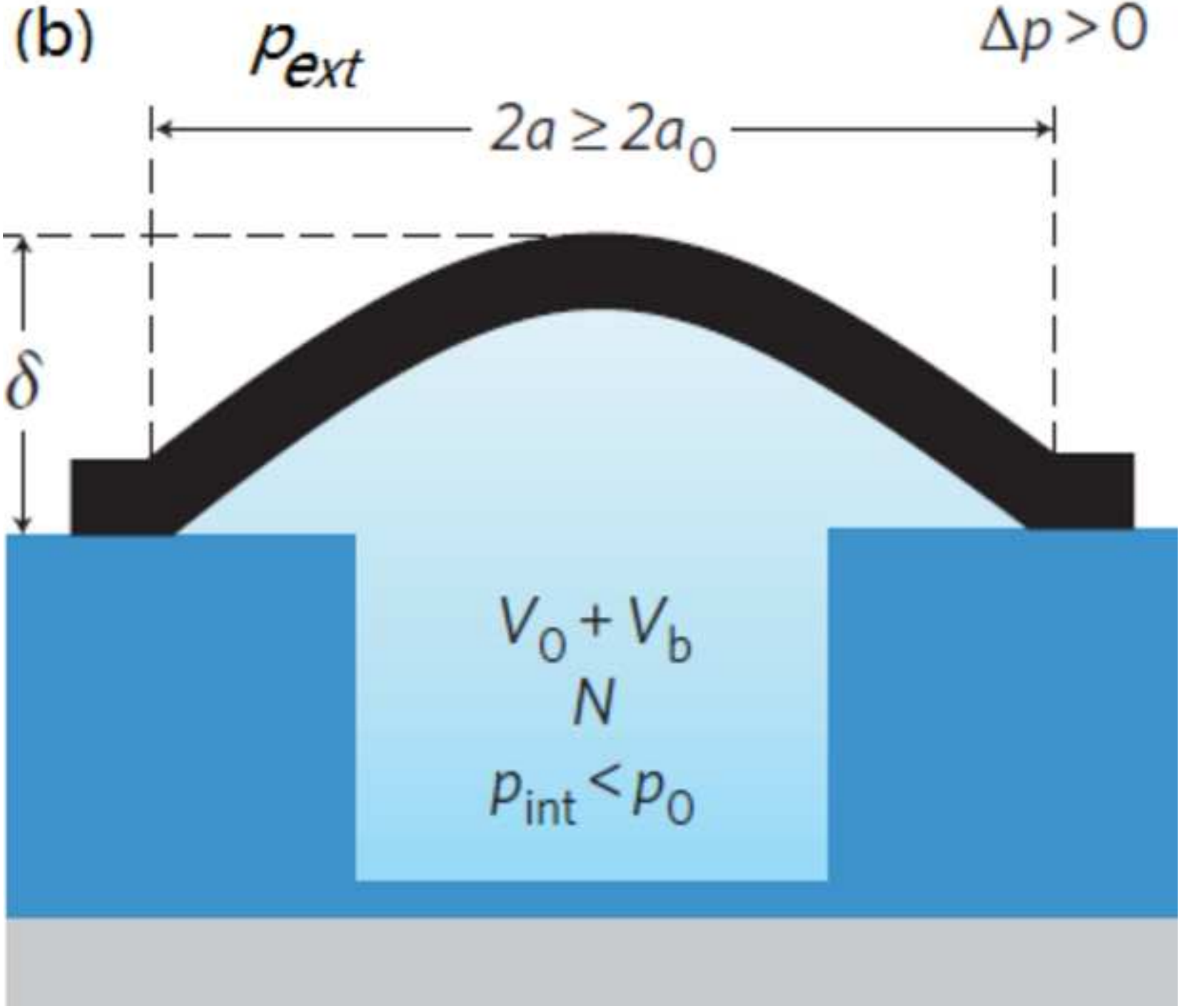

Figure(s)
Click here to download high resolution image

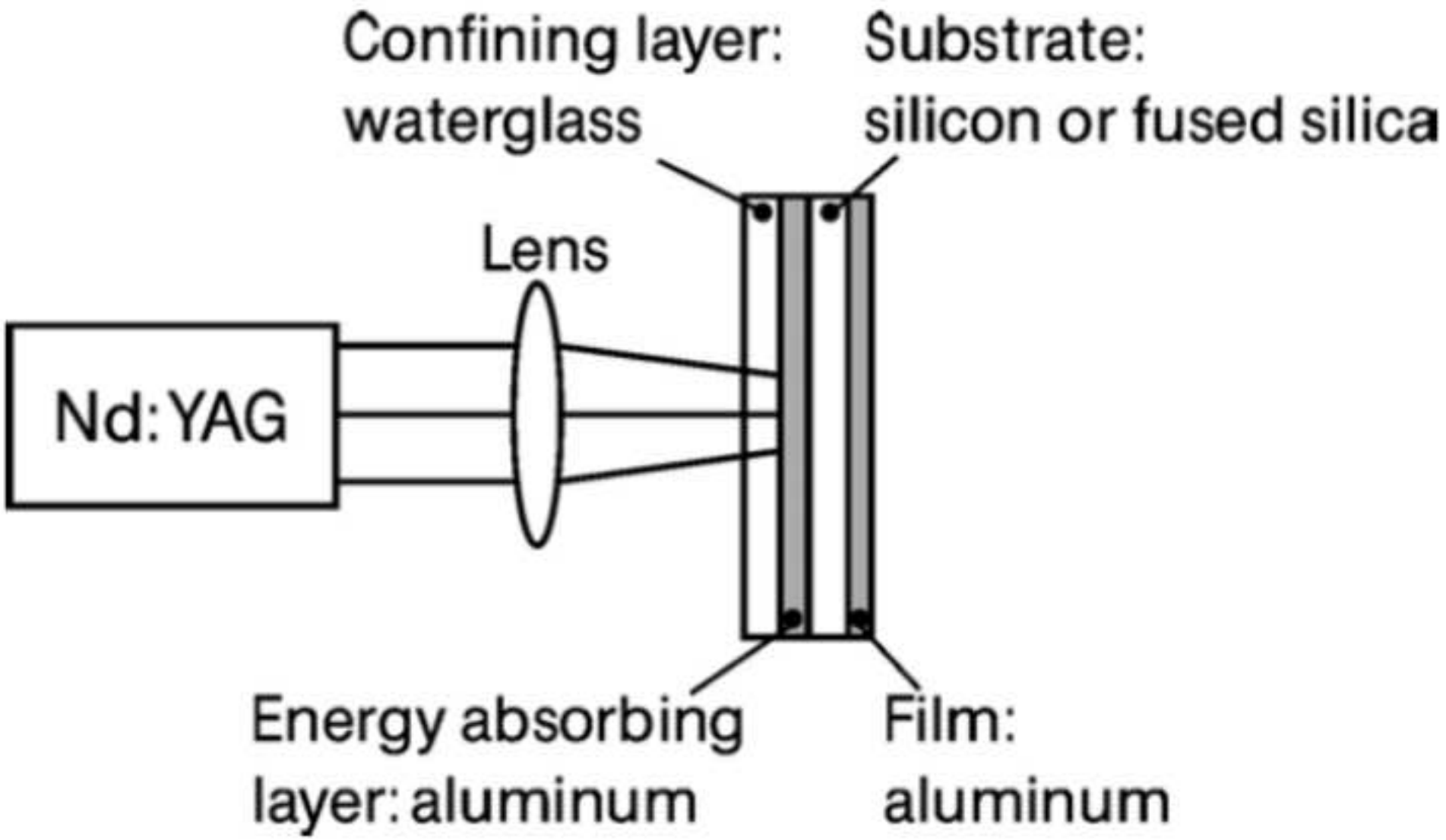

Figure(s)

Click here to download high resolution image

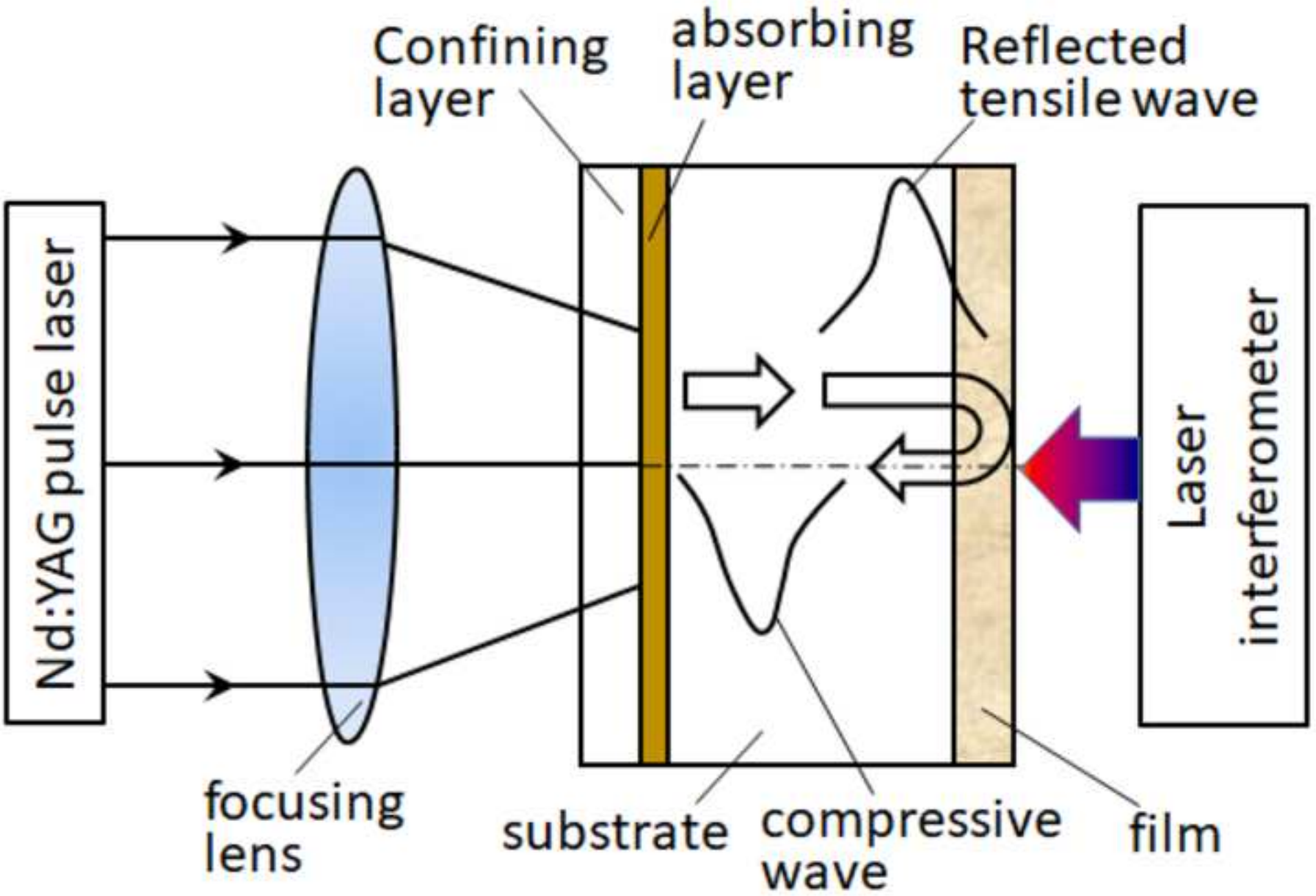

Figure(s)

Click here to download high resolution image

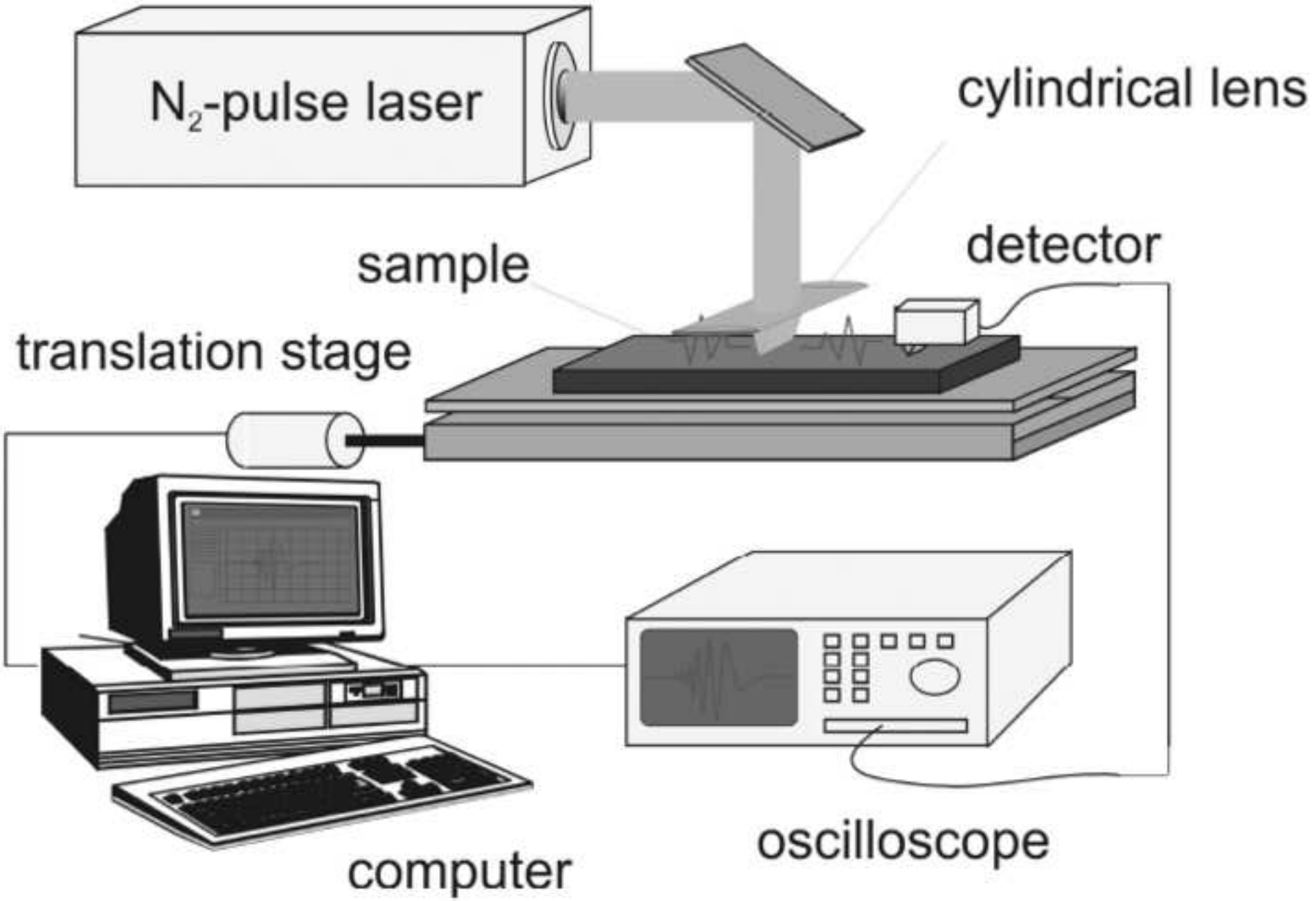

Figure(s)
Click here to download high resolution image

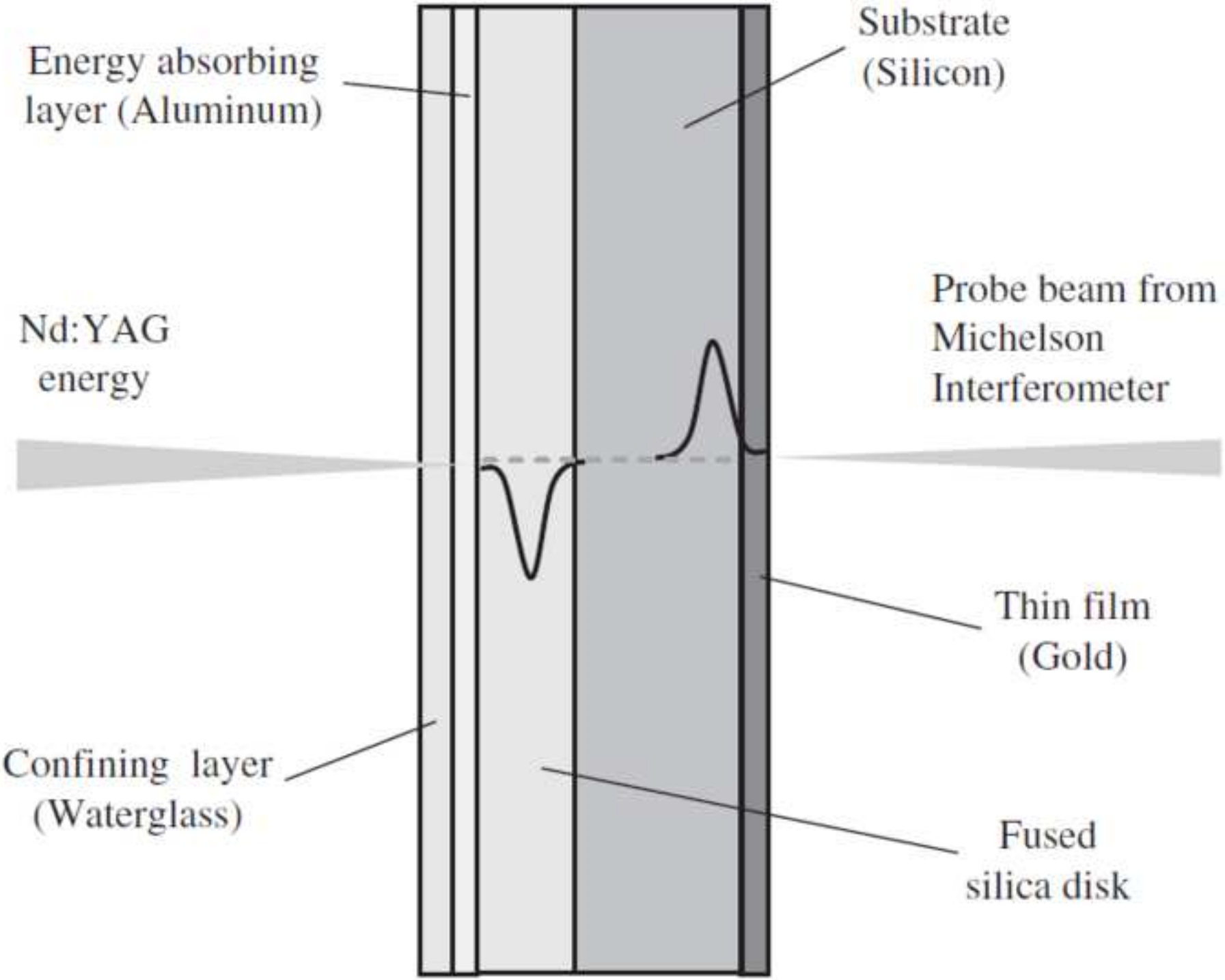

Figure(s)
Click here to download high resolution image

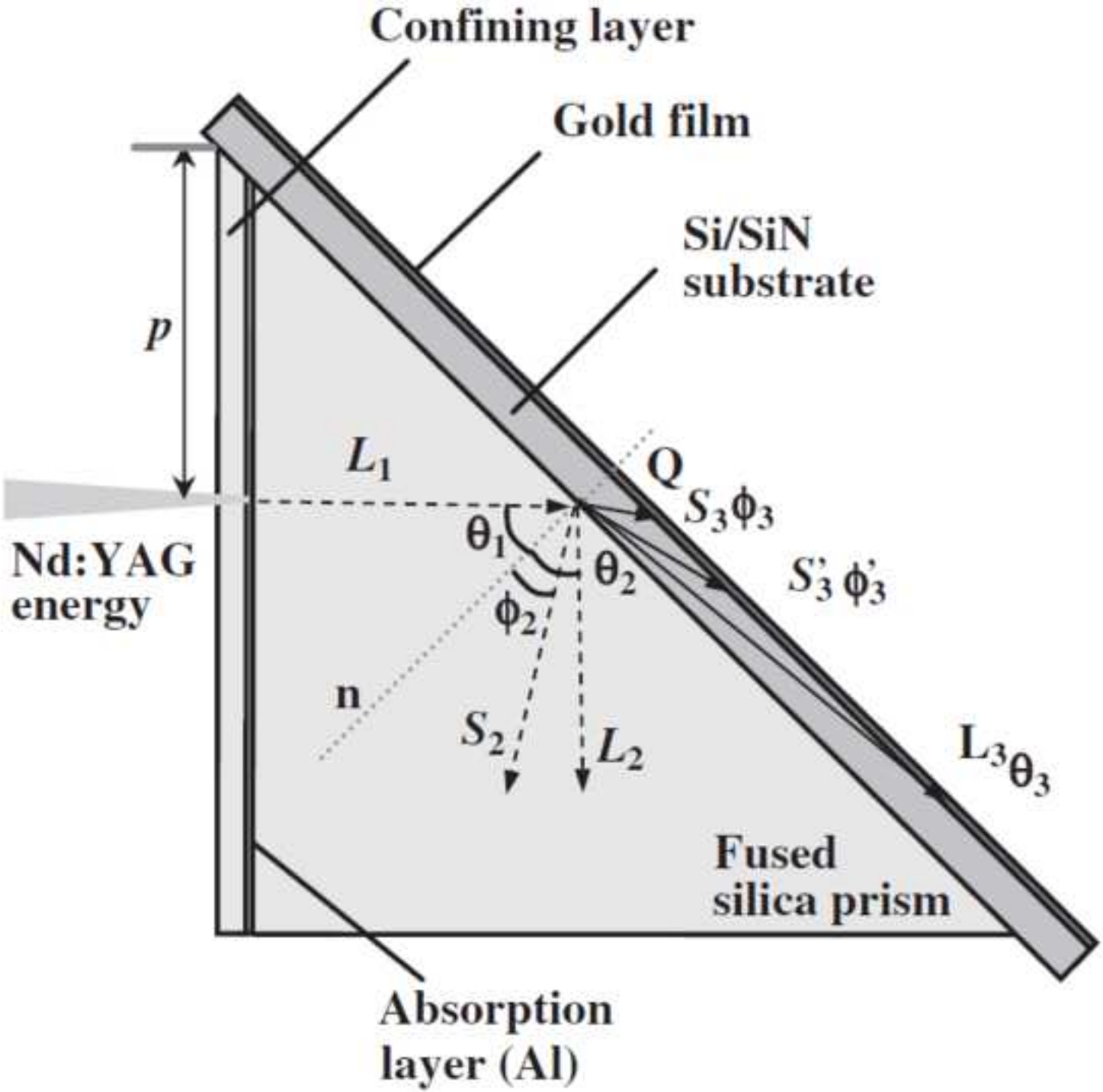

Figure(s)
Click here to download high resolution image

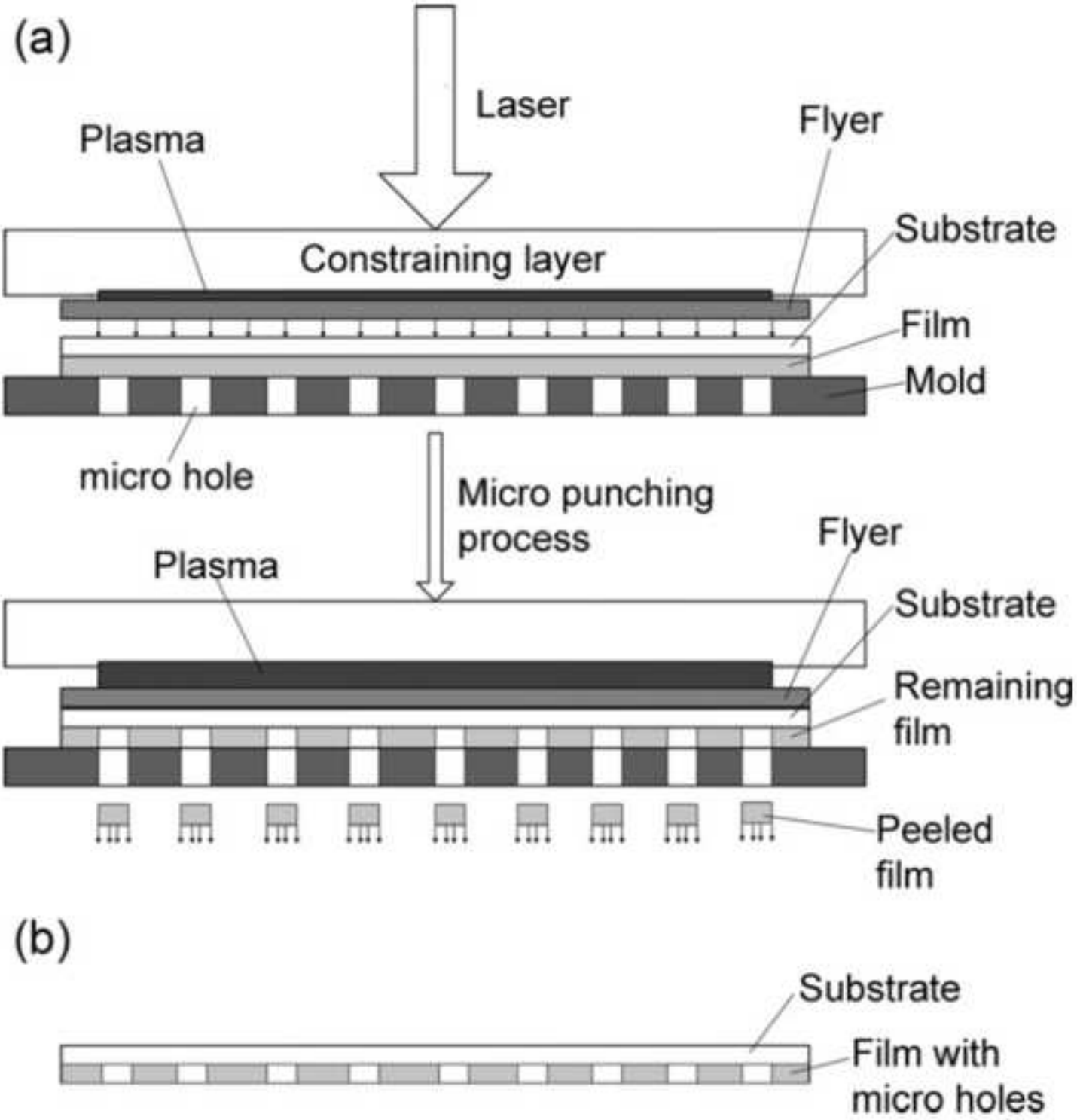

2019-03-11

Advances in test and measurement of the interface adhesion and bond strengths in coating-substrate systems, emphasising blister and bulk techniques

Chen, Xiaomei

Elsevier

Chen X, Shaw C, Gelman L, Grattan KTV. Advances in test and measurement of the interface adhesion and bond strengths in coating-substrate systems, emphasising blister and bulk techniques. Measurement, Volume 139, June 2019, pp. 387-402

https://doi.org/10.1016/j.measurement.2019.03.026